4

Weibull Weakest Link Theory Model for Bimodular Rectangular Flexural Specimens

4.1 Introduction

The testing, evaluation and prognosis of nuclear graphite components pose such an uncertainty of scattered damage accumulation patterns leading to catastrophic brittle fracture that probabilistic methods have evolved as an ultimatum to study their operational and functional transients, although low-impurity graphites are the most sought-after material for the fuel elements and moderator in Next Generation Nuclear Reactor (NGNR). The qualitative and quantitative accuracy, reproducibility, and reliability of test proceedings and results when correlated with the actual real-life problem of reactor components become dubious when a nuclear graphite specimen becomes excessively smaller or larger when compared to the standardized dimensions suggested by the ASTM standard. Such mitigating factors give an uncertainty of proper design postulations reflecting the low level of confidence among the research community within the spectrum of nuclear graphite applications. In most cases, the material selection based on outstanding physical properties such as high-temperature strength, erosion-corrosion, thermal shock resistance, low density and well established refractory properties for the sustainability of structural integrity of critical components leads to ceramic-based materials like graphite. However, the uncertainty of stochastic fracture behavior of

even near identical graphite components, the susceptibility to sustaining tensile stresses, low strain and fracture toughness arising out of the general problem of scattered flaws and brittleness results in compromising structures from the designer's perspective rather than tackling the problem efficiently. Many a cases, the different stress-strain behavior in tension and compression for such materials are rather avoided in design than solved by efficient analytical, numerical or experimental procedures. The acceptance of such hypothesis is reasoned to be simplifying the strength design, though we understand the fallacy of such assumptions shall only be magnified as we build up real structures of significantly large size than lab scale models. As the size and so the volume and/or surface area of the structure is scaled up, the probability of encountering severe flaws and their numbers are only increased. If the material is inherently brittle, catastrophic failure of such components are very intriguing to explain with existing classical unimodular assumptions. Therefore, there is a need for reassessment of such assumptions leading to closed form and semi-analytic solutions for an improved design. The endeavor of the present work has been to conduct a detailed analytical, numerical and experimental analysis of strength scaling of bimodular specimens with different geometry to eliminate the deficiencies associated with the existing model. Probabilistic approach based on the weakest link theory (WLT) model of Weibull distribution functions has been employed for evaluating effective volume and area by developing an analytic three-dimensional numerical model. Weibull functional parameters such as Weibull modulus and characteristics strength has been evaluated from tension and compression testing of flexural specimens with square cross-sectioned graphite specimens. The estimates from numerical simulation of the unimodular finite element model and

bimodular finite element model have been compared with calculations obtained from existing literatures (Quinn and Morrell 1991; Quinn 2003b, a; ASTM C1239 −13 2013; Bhushan et al. 2016) and CARES/Weibpar respectively (WeibPar V-4.3 and CARES V-9.3).

Bimodularity has been recognized as an uncertainty in the design and development of high-risk ceramic and graphite structures leading to catastrophic failure. This results in an asymmetric shifting of elastic axis and elastic surface from an otherwise neutral axis and neutral surface respectively, when the structure is mechanically loaded (Ambartsumyan 1969; Tabaddor 1972; Reddy et al. 1980; Reddy and Bert 1982; Reddy and Chao 1983; Kamiya 1987). Classical elasticity theory has limited application for these kinds of structural materials in its original form as it not only considers the elastic properties to be same in tension and compression, but also it does not take into account the material non-linearity. Early works by Saint Venant (Saint-Venant 1864) and Timoshenko (Timoshenko 1941) has postulated the concept of variation of elastic modulus for beams under flexural loading exhibiting bimodular characteristics even under simple bending. Structural integrity assessment of structures comprising of bimodular materials necessitates the evaluation of state of stress as an integral factor of tension and compression modulus following a rigorous iterative procedure, where numerical computations are very much involved even running into hundreds of thousands of steps for an acceptable convergence limit. In this regard, evaluation of only effective modulus are erroneous leading to a design handicap at the prototype stage, though it might give some initial estimate of bending and shear deformation with a unimodular constitutive relationship. Consequently, the influence of variation of structure behavior from test specimen geometry to actual structural

shape becomes highly exaggerated forcing the designer to take shelter under either over-designed/under-designed hypothetical safety factor. This might lead to huge material and volume loss, not to mention that the cost and reliability of the structure has been compromised. The redundancy observed in the existing literature to address those issues concentrating only on unimodular based reliability evaluation of effective volume and surface area parameters for test specimens has been the motivation of the present study. Expectedly, this has been a cause of worry in correlating the experimental observations with postulated design parameters for a bimodular based material structure. Though present endeavor to evaluate reliability parameters for analytical and numerical modeling of such real-life structural behavior might be uncannily computationally exhaustive, still we feel it will be worthy to get rid of such uncertainty of scaling of size and shape from laboratory specimen to actual prototype in high-risk design parts exhibiting stress dependent elasticity. The conversion of design data from one specimen configuration to another without concern of bimodularity effect and prior knowledge of flaw distribution leads to unexpected failure rendering the existing design principles very much conservative for such ceramic and nuclear grade graphite cladded structures in contrast to metals.

Graphite is currently being used for the construction of the major core components such as the fuel block, reflector, moderator and core support critical structure in a nuclear reactor. This will be a key material in the development of Very High-Temperature Reactor (VHTR) for the six next-generation nuclear reactor systems within the Generation IV International Forum ([CSL STYLE ERROR: reference with no printed form.]). The VHTR is considered to be the Next Generation Nuclear Reactor (NGNR) in the evolutionary development of

high-temperature gas-cooled reactors with significant advantage of inherent safety, high thermal efficiency, process heat application capability, low operation and maintenance costs, and modular construction(Srinivasan 2008, 2014; Nemeth and Bratton 2011; Chi 2013, 2015, 2016). Using appropriate ASTM standards, Weibull failure probability analysis for components is presented by M. Srinivasan, for strength specification for nuclear grade graphites for core components in advanced high-temperature gas-cooled reactors. The probability of fracture and reliability of large graphite blocks are calculated for different and discrete values of service tensile stresses (Srinivasan 2008). The pioneer research work in the field of size effect on strength in quasi-brittle material has been done by Bazant (Bazant and Kazemi 1990; Bazant and Xi 1992; Bazant et al. 1992; Bazant and Pang 2006). The scaling of unimodular strength of nuclear grade graphite has been studied by various researchers (Yoon et al. 2011; Hindley et al. 2012; Chi 2013, 2015).

It is very well known that in ceramic components, the size effect relative to tensile strength is fairly prominent. As the size of a component is increased, the tensile strength decreases. The reason is that as the volume or surface area of the component is increased, the chances of encountering a critical flaw with harmful orientations to the applied load increases. Thus, the calculation of effective volume and the effective surface is a key step in estimating the reliability of ceramic component life cycle. Most common tests performed to assess the strength and reliability of ceramic components are bend bar specimens tested in three-point and four-point flexure specimen under diametral compressive or tensile loads and biaxial ring-on-ring specimens. Weibull effective volumes and

surfaces are used to scale ceramic strength from one component size to another or from one loading configuration to another. The

Weibull weakest-link model leads to a strength dependency on component size (Quinn and Morrell 1991; Quinn 2003a, b; ASTM C1683-10 2010). When volume flaws predominate and if the distribution is a Weibull 2-parameter form, then stress state can be correlated with effective volume as follows

$$\frac{\sigma_1}{\sigma_2} = \left(\frac{V_{E2}}{V_{E1}} \right)^{1/m} \tag{4.1}$$

When surface flaws predominate and if the distribution is a Weibull 2-parameter form:

$$\frac{\sigma_1}{\sigma_2} = \left(\frac{A_{E2}}{A_{E1}} \right)^{1/m} \tag{4.2}$$

Where, σ_1, σ_2 are the mean strength of the specimen type 1 and 2 fabricated from same material; V_{E1}, V_{E2} are effective volumes of the specimen type 1 and 2; A_{E1}, A_{E2} are effective surfaces of the specimen type 1 and 2; m is Weibull modulus.

Even though the classical theory of elasticity assumes that materials have the same elastic properties in tension as well as in compression, numerous studies have indicated that materials like ceramic, composite and many other natural and artificial materials including nuclear grade graphite exhibit differently in tension and compression. Materials which exhibit different elastic moduli in tension and compression are known as bimodular materials, and in this paper, we consider those materials, which follow linear elastic fracture characteristics. With the developments of new materials, the numerical analyses incorporating the bimodular properties are gaining the attention of the researchers. The phenomena of different behavior in tension and compression were first recognized by Saint-

Venant in 1864 (Saint-Venant 1864); however, the concept did not receive much attention for a long time from the research community. Later on, the concept of a bimodular material was originated by Timoshenko (Timoshenko 1941), while considering the flexural stress in such a material undergoing pure bending. The effective modulus for stiffness of such a beam in pure bending was given by (Marin 1962). The bimodular concept was extended to two-dimensional materials by (Ambartsumyan 1965, 1966, 1969). Within the last few decades, several attempts have been made to establish constitutive relationships for such materials (Isabekian and Khachatryan 1969; Bert 1977, 1978; Green and Mkrtichian 1977). Also, a lot of literature related to analytical and numerical solutions is available for the effective volume and effective surface area in beams with single modulus (Nemeth et al. 1990b, 2012, 2013; Danzer 1992; Jain 2008). Though in the last few decades some numerical analyses for the structural problems have been done considering the bimodular behavior of the material, but the development of the analytical formula for computing the effective volumes, surfaces and strength scaling of bimodular material from lab scale to real scale has not been studied in detail for computational and experimental simplicity. In a nutshell, the reliability of structures comprising of bimodular material remains a challenging issue in high risk nuclear components.

Though analytical studies on unimodular material for rectangular and cylindrical specimens have been carried out by Quinn [1-3], however, to the best of the authors' knowledge the analytical expressions of scaling of the strength for bimodular material using Weibull effective volumes and surfaces are not reported in the literature so far. As the effective volume and the effective surface of bimodular material subjected to flexural loading are significantly changed by the

neutral axis shift, the chance of failure is also considerably affected. In the present work, expressions for the effective volume and effective surface for the rectangular and square beam graphite specimens subjected to various flexural loading configurations are tabulated in Table 1 for the strength scaling of structural components. As for the practical purposes, the reported results can be readily used to convert data rapidly between one loading configuration to another. Therefore, expressions of strength scaling ratios and table of conversion factors, for strength scaling from one flexural loading configuration to another with different Weibull modulus has also been provided in Table 2. For illustrative purposes, derivation of effective volumes and effective surfaces for two simple loading configurations are illustrated in this paper.

4.2. Weibull Effective Volume and Surface Area for Bimodular Material

This paper deals with the bimodular beam of rectangular cross-section with different flexural loading configurations. Figures 4.1, 4.2 and 4.3 represent respectively the four-point flexural specimen, three-point flexural specimen and the beam subjected to uniform bending.

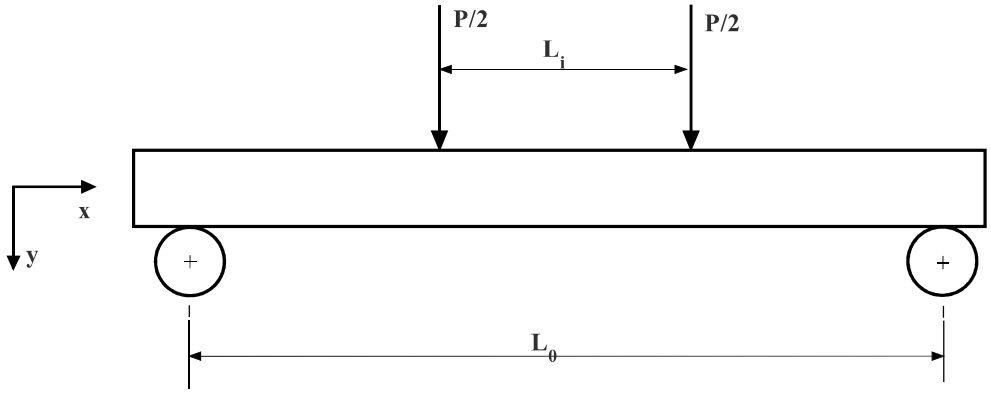

Fig. 4.1 Four-point flexure specimen

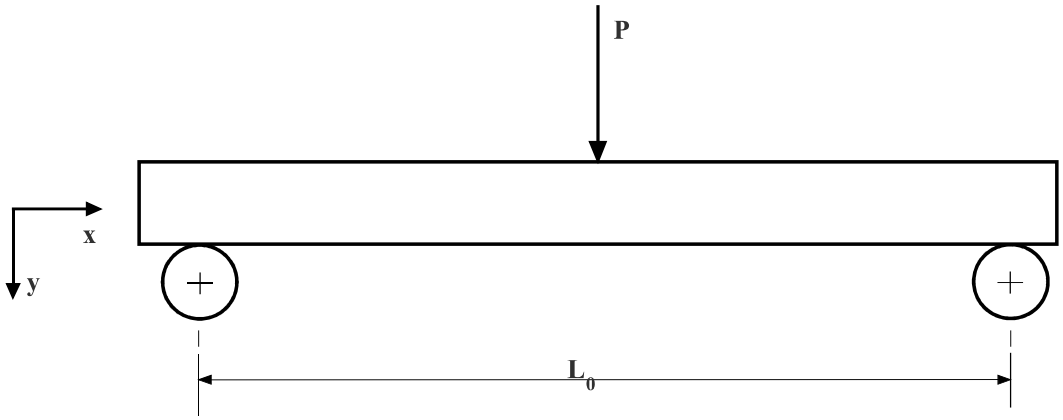

Fig. 4.**2** Three-point flexure specimen

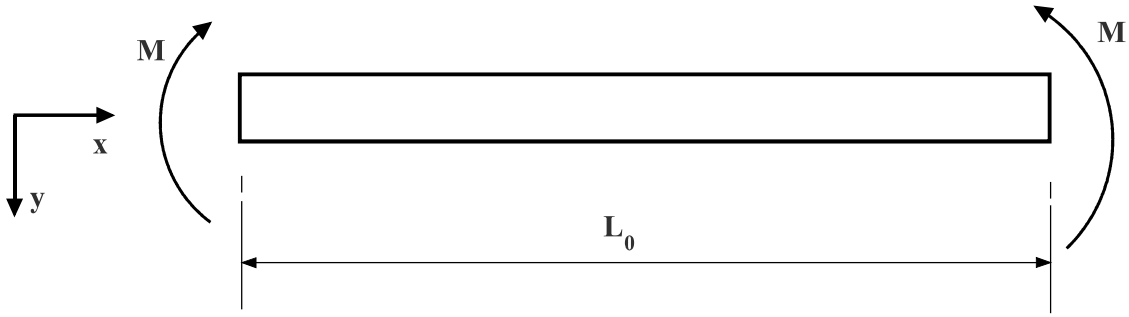

Fig. 4.**3** Beam subjected to uniform bending

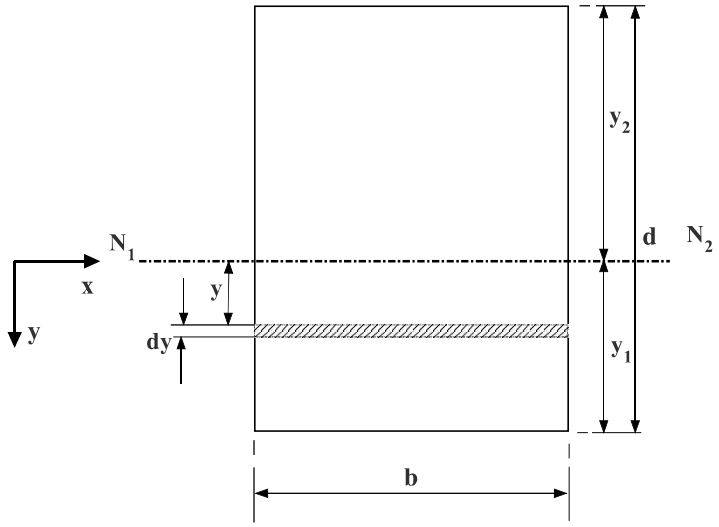

Fig. 4.4 The rectangular cross-section of a beam having elemental area dA at a distance of y from neutral axis N_1N_2

In order to derive the expression for effective volume, effective surface and after that strength scaling factor, the following cross-section of the rectangular beam has been considered, Fig. 4.4. In this figure, y_1 is the distance of the bottom surface, which is stressed in tension, from the neutral axis of the beam and it is evaluated by force balance at any plane perpendicular to the neutral axis:

$$\int_{-y_2}^{y_1} \sigma dA = 0 \tag{4.3}$$

$$\int_{0}^{y_1} \sigma_T dA = \int_{0}^{-y_2} \sigma_C dA \tag{4.4}$$

Using flexure formula, one can have

$$y_1 = \frac{1}{1+\sqrt{\alpha}} d \tag{4.5}$$

$$y_2 = -\frac{\sqrt{\alpha}}{1+\sqrt{\alpha}} d \tag{4.6}$$

Where, $\alpha = \frac{E_T}{E_C}$ is the ratio of elastic modulus in tension to compression, and d is the depth of the beam cross-section.

Now, taking moment about neutral axis lead to

$$M_x = \int_{0}^{-y_2} \sigma_C dA.y + \int_{0}^{y_1} \sigma_T dA.y \tag{4.7}$$

$$M_x = \frac{E_T b}{\rho}\left[-\frac{E_C}{E_T}\frac{y_2^3}{3} + \frac{y_1^3}{3}\right] \tag{4.8}$$

where the moment M_x can vary with position along the length (x-axis) $M_x = M(x)$ depending on if it is three point, four-point inner span, or between inner and outer.

Also, from Fig. 4.1, the maximum bending moment can be deduced as

$$M_{\max} = \left(\frac{P(L_0 - L_i)}{4} \right)$$

Now expressing the intensity of stress for the tension side yields

$$\sigma_T(x, y) = \frac{3M_x y\left(1+\sqrt{\alpha}\right)^2}{bd^3} \tag{4.9}$$

Weibull effective volume can be expressed as

$$V_{eff} = \int_V \left(\frac{\sigma_x}{\sigma_{\max}} \right)^m dV \tag{4.10}$$

The integration is performed overall volume (or surface) elements that have tension stress on them for the rectangular specimen. The resulting expression can be given as:

$$V_{eff} = \int_{x=0}^{L_0} \int_{y=0}^{y_1} \int_{z=0}^{b} \left(\frac{\sigma_x}{\sigma_{\max}} \right)^m dxdydz \tag{4.11}$$

In Eq. (4.1), the effective volume V_E is assumed to be the specimen volume V for direct uniform tensile loading, however in case of flexural loading due to the effect of stress gradient, effective volume $V_E < V$. The effective volume is the size of a hypothetical tension test specimen that when stressed to the same level as the test specimen in question has the same probability of fracture. In other words, a flexure bar of volume V is equivalent to a tensile specimen of size V_E (Quinn and Morrell 1991; Quinn 2003a, b; ASTM C1683-10 2010). So, in Eq. (4.11), the

integration is performed over the portion of the specimen that are stressed in tension.

4.2.1 Effective Volume for Four-Point Flexural Beam with Bimodular Property

Using the concept explained just before this subsection, the expression of the effective volume for four-point flexural beam, Fig. 4.1 with bimodular property is derived here. Employing the maximum bending moment for the figure and using Eq. (4.9), the maximum tensile stress in the specimen can be given as

$$\sigma_{T_{\max}} = \left(\frac{3P(L_0 - L_i)(1+\sqrt{\alpha})}{4bd^2} \right) \tag{4.12}$$

Now, the ratio of stress in the x-direction to the maximum tensile stress at any point in the volume of the specimen (stressed in tension) becomes

$$\frac{\sigma_T}{\sigma_{T_{\max}}} = \frac{\dfrac{3M_x y\left(1+\sqrt{\alpha}\right)^2}{bd^3}}{\left(\dfrac{3P(L_0 - L_i)(1+\sqrt{\alpha})}{4bd^2} \right)} \tag{4.13}$$

Substituting the above expression in the expression of the effective volume, Eq. (4.10) leads to

$$V_{eff} = 2\int_{y=0}^{y_1}\int_{x=0}^{L_0/2}\left(\frac{4M_x y(1+\sqrt{\alpha})}{P(L_0 - L_i)d} \right)^m dxdy \int_{z=0}^{b} dz \tag{4.14}$$

After simplification,

$$V_{eff} = 2b \int_{x=0}^{L_0/2} \left(\frac{4M_x(1+\sqrt{\alpha})}{P(L_0 - L_i)d} \right)^m dx \int_{y=0}^{y_1} y^m dy \tag{4.15}$$

Simplifying further

$$V_{eff} = \frac{2b}{m+1} \left(\frac{d}{1+\sqrt{\alpha}} \right) \left(\left(\left(\frac{d}{1+\sqrt{\alpha}} \right) \frac{4(1+\sqrt{\alpha})}{P(L_0 - L_i)d} \right)^m \right) \int_{x=0}^{L_0/2} (M_x)^m .dx \tag{4.16}$$

Finally,

$$V_{eff} = \frac{2b}{m+1} \left(\frac{d}{1+\sqrt{\alpha}} \right) \left(\frac{\left(L_0 - L_i + (m+1)L_i\right)}{2(m+1)} \right) \tag{4.17}$$

or

$$V_{eff} = V_B \left(\frac{1}{1+\sqrt{\alpha}} \right) \left(\frac{\left(1 + m\left(L_i / L_0\right)\right)}{(m+1)^2} \right) \tag{4.18}$$

Here it is noted that $V_B = bdL_0$ is the volume within the outer support spans, not the entire volume including the overhang. For three-point flexural specimen as shown in Fig. 4.2, one can find the expression for effective volume after putting $L_i = 0$ as

$$V_{eff} = V_B \left(\frac{1}{1+\sqrt{\alpha}} \right) \left(\frac{1}{(m+1)^2} \right) \tag{4.19}$$

4.2.2 *Effective Volume for Beam Subjected to Uniform Bending with Bimodular Property*

Approaching in a similar way like the 4-point bend specimen, now in case of beam subjected to uniform bending having constant bending moment *M*, Fig. 4.3, taking a moment about neutral axis yields

$$M = \frac{E_T bd^3}{3\rho}\left(\frac{1}{\left(1+\sqrt{\alpha}\right)^2}\right) \tag{4.20}$$

Subsequently, tensile stress at a point in the specimen is given by

$$\sigma_T = \frac{3M\left(1+\sqrt{\alpha}\right)^2}{bd^3} y \tag{4.21}$$

And the expression of maximum tensile stress in the component can be given by

$$\sigma_{T_{\max}} = \frac{3M\left(1+\sqrt{\alpha}\right)}{bd^2} \tag{4.22}$$

So, the effective volume expression in case of uniform bending, using Eqs. (4.21) and (4.22) in Eq. (4.9), is given by

$$V_{eff} = \int_V \left(\frac{\frac{3M\left(1+\sqrt{\alpha}\right)^2}{bd^3} y}{\frac{3M\left(1+\sqrt{\alpha}\right)}{bd^2}} \right)^m dV \tag{4.23}$$

Or

$$V_{eff} = 2\int_{x=0}^{L_0/2}\int_{y=0}^{y_1}\int_{z=0}^{b}\left(\frac{\left(1+\sqrt{\alpha}\right)}{d} y\right)^m dxdydz \tag{4.24}$$

After simplification, the above expression leads to

$$V_{eff} = \left[\frac{V_B}{\left(m+1\right)\left(1+\sqrt{\alpha}\right)}\right] \tag{4.25}$$

where $V_B = bdL_0$

4.2.3 Effective Surface Area for Four-Point Flexural Beam with Bimodular Property

The formula of Weibull effective surface can be put as following (ASTM C1683-10 2010)

$$A_{eff} = \int_A \left(\frac{\sigma}{\sigma_{\max}} \right)^m dA \tag{4.26}$$

Differential element is shown in Fig. 4.5, and it can be written as

$$dA = dx\left(dy + dz\right)$$

Incorporating the expressions of σ and σ_{max} , i. e. using Eq. (13) in Eq. (26), we have

$$A_{eff} = 2\left(2\int_{x=0}^{L_0/2}\int_{y=0}^{y_1}\left(\frac{4M_x y\left(1+\sqrt{\alpha}\right)}{Pd(L_0 - L_i)} \right)^m dydx + \int_{x=0}^{L_0/2}\left(\int_{z=0}^{b}\left(\frac{4M_x y\left(1+\sqrt{\alpha}\right)}{Pd(L_0 - L_i)} \right)^m dz \right) dx \right) \tag{4.27}$$

From the limits of the integration one should be sure that the integration is carried out here is only for the tensile loaded surfaces.

On rearranging:

$$A_{eff} = 2\left[2\left(\frac{4\left(1+\sqrt{\alpha}\right)}{Pd(L_0 - L_i)} \right)^m \int_{x=0}^{L_0} \left(M_x\right)^m dx \left(\int_{y=0}^{y_1} y^m dy \right) + \left(\frac{4y_1\left(1+\sqrt{\alpha}\right)}{Pd(L_0 - L_i)} \right)^m \int_{x=0}^{L_0} \left(M_x\right)^m dx \left(\int_{z=0}^{b} dz \right) \right] \tag{4.28}$$

After substituting the expression of bending moment for Fig. 4.1; approaching in a similar way as done for the effective volume, the above equation turns out to be:

$$A_{eff} = L_0\left[\frac{2}{m+1}\left(\frac{d}{1+\sqrt{\alpha}}\right)+b\right]\left(\frac{\left(1+m(L_i/L_0)\right)}{(m+1)}\right) \tag{4.29}$$

For 3 point flexural specimen, the effective area expression leads to

$$A_{eff} = L_0\left[\frac{2}{m+1}\left(\frac{d}{1+\sqrt{\alpha}}\right)+b\right]\left(\frac{1}{(m+1)}\right) \tag{4.30}$$

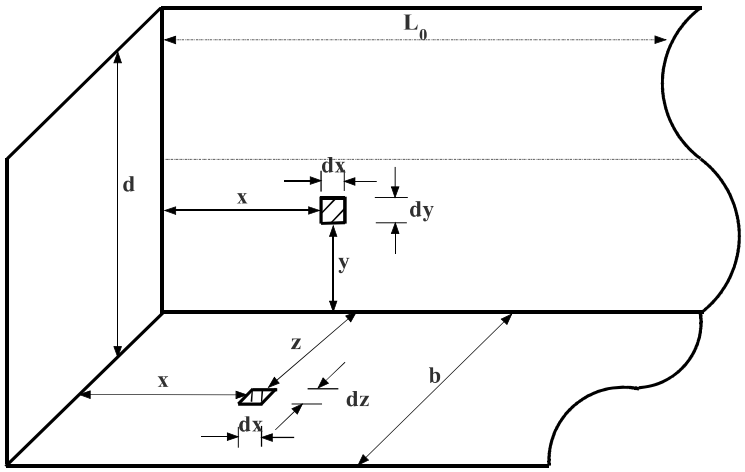

Fig. 4.5 Differential elements

4.2.4 Effective Surface Area for Beam Subjected to Uniform Bending with Bimodular Property

Substituting the ratio of tensile stress to maximum tensile stress i. e. using Eqs. (4.21) and (4.22) in Eq. (4.26) one gets:

$$A_{eff} = 2\left[2\int_{x=0}^{L_0/2}\int_{y=0}^{y_1}\left(\frac{\left(1+\sqrt{\alpha}\right)}{d}y\right)^m dxdy + \int_{x=0}^{L_0/2}\int_{z=0}^{b}\left(\frac{\left(1+\sqrt{\alpha}\right)}{d}y\right)^m dxdz\right]$$

After simplification,

$$A_{eff} = 2\left[\left(\frac{\left(1+\sqrt{\alpha}\right)}{d}\right)^{m}\left(2\int_{x=0}^{L_0/2}\left(\int_{y=0}^{y_1}(y)^m\,dy\right)dx + \int_{x=0}^{L_0/2}\left(\int_{z=0}^{b}dz\right)(y)^m\,dx\right)\right] \tag{4.31}$$

And finally, the expression for effective area turns out to be

$$A_{eff} = \left[\left(\left(\frac{2d}{\left(1+\sqrt{\alpha}\right)(m+1)}\right)+b\right)L_0\right] \tag{4.32}$$

Table 4.1(a) Formulas for Effective Volumes for Rectangular Beams loaded in Flexure for bimodular specimens

Sl. No.	Configuration	Effective Volume, V_{eff}
1	Uniform bending	$V_{eff} = V_B\left[\frac{1}{(m+1)\left(1+\sqrt{\alpha}\right)}\right]$
2.	Three-point	$V_{eff} = V_B\left(\frac{1}{1+\sqrt{\alpha}}\right)\left(\frac{1}{(m+1)^2}\right)$
3.	Four-point General	$V_{eff} = V_B\left(\frac{1}{1+\sqrt{\alpha}}\right)\left(\frac{(1+mN)}{(m+1)^2}\right)$
4.	Four-point,1/4 point, (Fig. 4.6)	$V_{eff} = \frac{V_B}{2}\left(\frac{1}{1+\sqrt{\alpha}}\right)\left(\frac{(2+m)}{(m+1)^2}\right)$
5.	Four-point,1/3 point, (Fig. 4.7)	$V_{eff} = \frac{V_B}{3}\left(\frac{1}{1+\sqrt{\alpha}}\right)\left(\frac{(3+m)}{(m+1)^2}\right)$

Table 4.1 (b) Formulas for Effective Surfaces for Rectangular Beams loaded in Flexure for bimodular specimens

Sl. No.	Configur-ation	Effective Area, A_{eff}	
		Rectangular	Square
1	Uniform bending	$A_{eff} = L_0\left[\left(\frac{2d}{\left(1+\sqrt{\alpha}\right)(m+1)}\right)+b\right]$	$A_{eff} = \frac{S}{4}\left[\left(\frac{2}{\left(1+\sqrt{\alpha}\right)(m+1)}\right)+1\right]$
2.	Three-point	$A_{eff} = L_0\left[\frac{2}{m+1}\left(\frac{d}{1+\sqrt{\alpha}}\right)+b\right]\left(\frac{1}{(m+1)}\right)$	$A_{eff} = \frac{S}{4}\left[\frac{2}{m+1}\left(\frac{1}{1+\sqrt{\alpha}}\right)+1\right]\left(\frac{1}{(m+1)}\right)$
3.	Four-point General	$A_{eff} = L_0\left[\frac{2}{m+1}\left(\frac{d}{1+\sqrt{\alpha}}\right)+b\right]\left(\frac{(1+mN)}{(m+1)}\right)$	$A_{eff} = \frac{S}{4}\left[\frac{2}{m+1}\left(\frac{1}{1+\sqrt{\alpha}}\right)+1\right]\left(\frac{(1+mN)}{(m+1)}\right)$
4.	Four-point,1/4 point,	$A_{eff} = L_0\left[\frac{2}{m+1}\left(\frac{d}{1+\sqrt{\alpha}}\right)+b\right]\left(\frac{(2+m)}{2(m+1)}\right)$	$A_{eff} = \frac{S}{8}\left[\frac{2}{m+1}\left(\frac{1}{1+\sqrt{\alpha}}\right)+1\right]\left(\frac{(2+m)}{(m+1)}\right)$
5.	Four-point,1/3 point,	$A_{eff} = L_0\left[\frac{2}{m+1}\left(\frac{d}{1+\sqrt{\alpha}}\right)+b\right]\left(\frac{(3+m)}{3(m+1)}\right)$	$A_{eff} = \frac{S}{12}\left[\frac{2}{m+1}\left(\frac{1}{1+\sqrt{\alpha}}\right)+1\right]\left(\frac{(3+m)}{(m+1)}\right)$

Please note that $N = L_i / L_0$; and total surface area $S = \left(2b\,L_0 + 2d\,L_0\right)$; these formulas all are consistent with the solutions reported by Quinn (Quinn 2003b), for the case of $\alpha = 1$ (Unimodular).

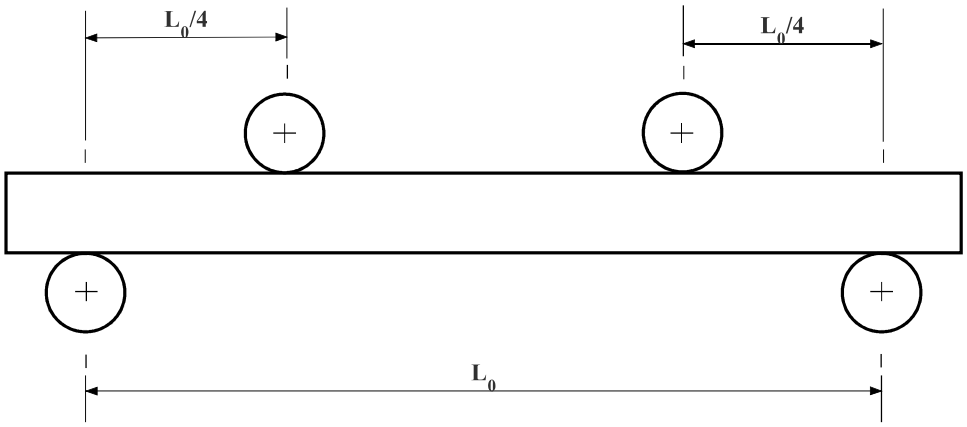

Fig. 4.6 Four-point 1/4 point flexure specimen

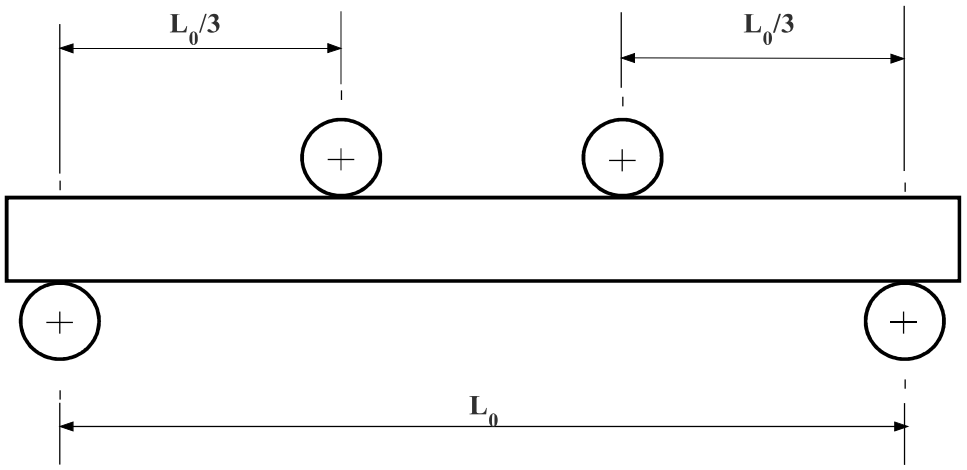

Fig. 4.7 Four-point 1/3 point flexure specimen

4.3. Strength Scaling

Strength scaling in case of flexural cylindrical and rectangular uni-modular material specimen loaded in three-point and four-point flexural loading, in the present section strength scaling ratios for flexural rectangular specimen with bi-modular property for both surface and volume flaw distribution have been provided (Quinn and Morrell 1991; Quinn 2003a, b; ASTM C1683-10 2010).

Strength scaling ratios are derived below for the conversion of strengths among the various flexural loading configurations.

When volume distributed flaws dominate, strength scaling ratio for the four-point 1/3 point flexural strength to the four-point 1/4 point flexural strength, is

$$\frac{\sigma_{4\,pt,30}}{\sigma_{4\,pt,40}} = \left(\frac{V_{E,4\,pt,40}}{V_{E,4\,pt,30}}\right)^{1/m} = \left[\frac{\frac{V_{4\,pt,40}}{2}\left(\frac{1}{1+\sqrt{\alpha}}\right)\left(\frac{(2+m)}{(m+1)^2}\right)}{\frac{V_{4\,pt,30}}{3}\left(\frac{1}{1+\sqrt{\alpha}}\right)\left(\frac{(3+m)}{(m+1)^2}\right)}\right]^{1/m} \tag{4.33}$$

Simplifying,

$$\frac{\sigma_{4\,pt,30}}{\sigma_{4\,pt,40}} = \left[\frac{L_{4\,pt,40}b_1d_1}{L_{4\,pt,30}b_2d_2}\frac{3(2+m)}{2(3+m)}\right]^{1/m} \tag{4.34}$$

If the cross-sections are the same, and substituting 40 mm or 30 mm for $L_{4\,pt,40}$ and $L_{4\,pt,30}$ respectively, the strength ratio becomes:

$$\frac{\sigma_{4\,pt,30}}{\sigma_{4\,pt,40}} = \left[\frac{2(2+m)}{(3+m)}\right]^{1/m} \tag{4.35}$$

This is the same outcome reported by Quinn, (Eq. 6, in (Quinn 2003b)), but here it is extended to the more general bimodular case.

In a similar way, when surface distributed flaws dominates, strength scaling depends on effective surface area of the specimen and the ratio is

$$\frac{\sigma_{4\,pt,30}}{\sigma_{4\,pt,40}} = \left(\frac{A_{E,4\,pt,40}}{A_{E,4\,pt,30}}\right)^{1/m} = \left[\frac{L_{4\,pt,40}\left[\frac{2}{m+1}\left(\frac{d}{1+\sqrt{\alpha}}\right)+b\right]\left(\frac{(2+m)}{2(m+1)}\right)}{L_{4\,pt,30}\left[\frac{2}{m+1}\left(\frac{d}{1+\sqrt{\alpha}}\right)+b\right]\left(\frac{(3+m)}{3(m+1)}\right)}\right]^{1/m}$$

For same cross sections the above ratio turns out to be

$$\frac{\sigma_{4\,pt,30}}{\sigma_{4\,pt,40}} = \left[\frac{2\left(2+m\right)}{\left(3+m\right)}\right]^{1/m} \tag{4.36}$$

Therefore, it can be observed here that the strength scaling ratios for the four-point 1/3 point flexural strength to the four-point 1/4 point flexural strength are identical, irrespective of the flaw distribution in the specimen provided that the cross-section remains the same. Expressing this as a function of conversion factor one can have the following expression

$$\frac{\sigma_{4\,pt,30}}{\sigma_{4\,pt,40}} = \left(\frac{V_{E,4\,pt,40}}{V_{E,4\,pt,30}}\right)^{1/m} = \left(\frac{A_{E,4\,pt,40}}{A_{E,4\,pt,30}}\right)^{1/m} = \left[\frac{2\left(2+m\right)}{\left(3+m\right)}\right]^{1/m} = W_1 \tag{4.37}$$

The values of W_1 are consistent with Quinn's W values in (Quinn 2003b) for the same case, but for materials with a constant elastic modulus.

Approaching in a similar way, strength scaling ratio for three-point flexural strength to the four-point 1/3 point flexural strength can be derived as

$$\frac{\sigma_{3\,pt,30}}{\sigma_{4\,pt,30}} = \left(\frac{V_{E,4\,pt,30}}{V_{E,3\,pt}}\right)^{1/m} = \left(\frac{A_{E,4\,pt,30}}{A_{E,3\,pt}}\right)^{1/m} = \left[\frac{3+m}{3}\right]^{1/m} = W_2 \tag{4.38}$$

And the same for the three-point flexural strength to the four-point 1/4 point flexural strength can be expressed as

$$\frac{\sigma_{3\,pt,40}}{\sigma_{4\,pt,40}} = \left(\frac{V_{E,4\,pt,40}}{V_{E,3\,pt}}\right)^{1/m} = \left(\frac{A_{E,4\,pt,40}}{A_{E,3\,pt}}\right)^{1/m} = \left[\frac{2+m}{2}\right]^{1/m} = W_3 \tag{4.39}$$

Table 4.2: Conversion factor for converting strengths among four-point and three-point flexure specimens with the same cross-section sizes tested on 10 mm x 30 mm fixture and 20 mm x 40 mm fixture as a function of the Weibull Modulus.

Weibull Modulus (*m*)	Conversion factor		
	W_1	W_2	W_3
5	1.11843	1.21673	1.28474
6	1.10064	1.20094	1.25992
7	1.08760	1.18767	1.239703
8	1.07759	1.17634	1.22284
9	1.06967	1.16653	1.20854
10	1.06323	1.15793	1.19623
12	1.05339	1.14353	1.17605
15	1.04331	1.12688	1.15335
20	1.03297	1.10721	1.12738
25	1.02662	1.09346	1.10972
30	1.02232	1.08321	1.09682

4.4. Weibull Analysis of Unimodular and Bimodular Flexural Graphite Specimens

The average tensile Young's Modulus of elasticity E_T = 8.502 GPa and the average compressive Young's Modulus of elasticity E_C = 5.618 GPa were evaluated according to ASTM E111 − 04 (ASTM E111-04 2010) as already mentioned in chapter 3. The average Modulus of elasticity are the average value for all twenty specimens tested in tension and compression as demonstrated in literature. The tensile and compressive specimens are prepared from the cuboidal shape graphite log of size as 1040x650x350mm^3 and cut down in the way that it occupies horizontal orientation (against gravity) as shown in Fig. 3.4. The modulus of elasticity in tension and compression are evaluated for these samples in horizontal orientation. The 180 small (100x10x10 mm^3) and 90 large specimens

(250x25x25 mm^3) are cut down from the same log in horizontal oriented (against gravity) for testing in different loading conditions. Two different sizes of flexural specimens are tested for characterizing the size effect on the strength as shown in Fig. 4.8 and Fig 4.9. Both types of specimens have square cross-section with same width-length ratio. The length of large and small size specimen is 250mm and 100mm respectively whereas the width of the specimen is 25mm and 10mm respectively. The outer and inner loading span are tabulated for three-point bend test and four-point bend test specimens in Table 4.3. These experiments help to characterize the size effect in nuclear grade graphite subjected to different loading conditions.

Table 4.3: Cylindrical loading span specifications for flexural specimen

Flexural Loading condition	Size	Outer span (mm)	Inner span (mm)	Specimen Tested
Three point bend specimen (ASTM: D7972-14)	Small	80	0	60
	Large	200	0	30
Four Point Bend 1/3 loading (ASTM: C651-13)	Small	78	26	60
	Large	195	65	30
Four Point Bend 1/4 loading (ASTM: C651-13)	Small	80	40	60
	Large	200	100	30

Fig. 4.8 Total 180 Small flexural specimens of square cross-section before testing

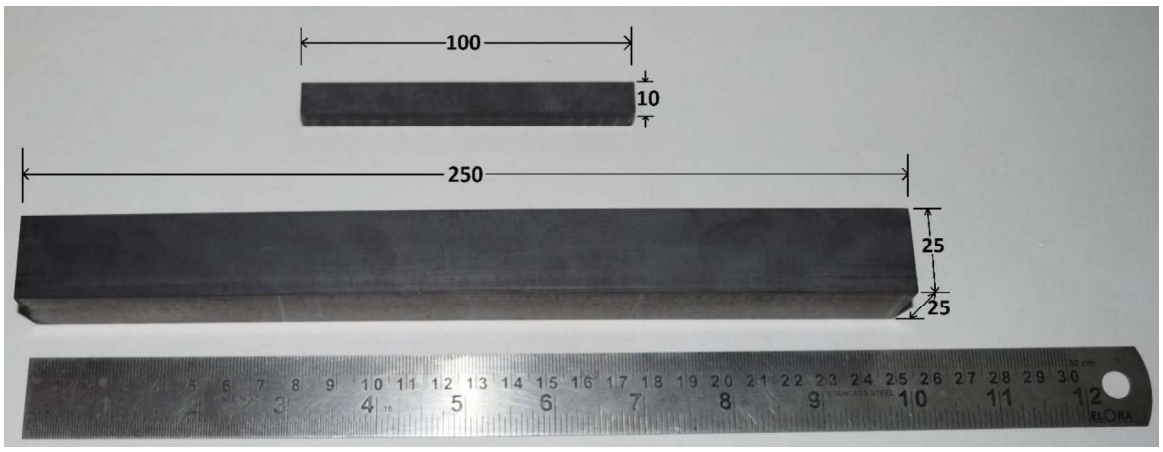

Fig. 4.9 Small and large size flexural specimens having square cross-section.

Figs. 4.10-4.12 show the testing arrangement for small and large flexural specimens. The three-point loading for large and small specimens have been presented in Fig. 4.10(a) and 4.10(b) respectively. The unimodular and bimodular strength is calculated for three-point bend test with following expression for three-point loading condition:

$$\sigma_{u3pbt} = \left(\frac{3PL_0}{2bd^2} \right) \qquad \text{(Unimodular strength)} \qquad (4.40)$$

$$\sigma_{b3pbt} = \left(\frac{3PL_0(1+\sqrt{\alpha})}{4bd^2} \right) \qquad \text{(Bimodular strength)} \qquad (4.41)$$

Unimodular and bimodular strength is calculated from the peak load obtained from the experimental testing. The results of sixty small and thirty large specimens are tabulated in the Table 4.4 and Table 4.5.

(a) (b)

Fig. 4.10 Testing arrangement of flexural specimens having square cross-section applied to three point bend loading (a) Large size and (b) Small size specimen.

Similarly, Fig. 4.11(a) illustrates fixture-specimen arrangement for four point bend test with 1/3 loading for large specimen whereas Fig. 4.11(b) depicts the same for small flexural specimen. The unimodular and bimodular strengths are calculated for four point bend test with 1/3 loading using following expression:

$$\sigma_{u3pbt} = \left(\frac{PL_0}{bd^2} \right) \qquad \text{(Unimodular strength)} \qquad (4.42)$$

$$\sigma_{b3pbt} = \left(\frac{PL_0(1+\sqrt{\alpha})}{2bd^2} \right) \qquad \text{(Bimodular strength)} \qquad (4.43)$$

Table 4.4: Experimental test results for small three-point bend specimen

Specimen No.	Peak load (N)	Unimodular Strength (MPa)	Bimodular Strength (MPa)	Specimen No.	Peak load (N)	Unimodular Strength (MPa)	Bimodular Strength (MPa)
Sample1	286.37	34.3644	38.2960	Sample31	283.12	33.9744	37.86142
Sample2	275.12	33.0144	36.79159	Sample32	309.73	37.1676	41.41996
Sample3	285.91	34.3092	38.23453	Sample33	305.12	36.6144	40.80346
Sample4	276.12	33.1344	36.92532	Sample34	304.32	36.5184	40.69648
Sample5	295.76	35.4912	39.55176	Sample35	325.55	39.066	43.53555
Sample6	299.46	35.9352	40.04656	Sample36	302.14	36.2568	40.40495
Sample7	306.11	36.7332	40.93586	Sample37	305.45	36.654	40.84759
Sample8	287.75	34.53	38.48059	Sample38	314.85	37.782	42.10465
Sample9	316.21	37.9452	42.28652	Sample39	292.65	35.118	39.13586
Sample10	296.58	35.5896	39.66142	Sample40	301.93	36.2316	40.37687
Sample11	307.11	36.8532	41.06959	Sample41	299.98	35.9976	40.1161
Sample12	304.51	36.5412	40.72189	Sample42	298.65	35.838	39.93824
Sample13	270.74	32.4888	36.20585	Sample43	319.76	38.3712	42.76126
Sample14	306.31	36.7572	40.9626	Sample44	307.56	36.9072	41.12976
Sample15	303.91	36.4692	40.64165	Sample45	293.76	35.2512	39.2843
Sample16	291.76	35.0112	39.01684	Sample46	309.63	37.1556	41.40658
Sample17	311.23	37.3476	41.62055	Sample47	315.04	37.8048	42.13006
Sample18	283.32	33.9984	37.88817	Sample48	321.76	38.6112	43.02872
Sample19	313.76	37.6512	41.95888	Sample49	311.43	37.3716	41.6473
Sample20	279.32	33.5184	37.35325	Sample50	294.65	35.358	39.40332
Sample21	313.76	37.6512	41.95888	Sample51	310.58	37.2696	41.53363
Sample22	300.53	36.0636	40.18965	Sample52	322.43	38.6916	43.11832
Sample23	301.94	36.2328	40.37821	Sample53	317.45	38.094	42.45235
Sample24	294.55	35.346	39.38995	Sample54	308.92	37.0704	41.31164
Sample25	284.65	34.158	38.06603	Sample55	317.57	38.1084	42.46839
Sample26	308.26	36.9912	41.22337	Sample56	312.21	37.4652	41.7516
Sample27	297.25	35.67	39.75101	Sample57	310.76	37.2912	41.5577
Sample28	318.76	38.2512	42.62753	Sample58	314.97	37.7964	42.1207
Sample29	297.47	35.6964	39.78044				
Sample30	302.25	36.27	40.41966				

Table 4.5: Experimental test results for large three-point bend specimen

Specimen No.	Peak load (N)	Unimodular Strength (MPa)	Bimodular Strength (MPa)	Specimen No.	Peak load (N)	Unimodular Strength (MPa)	Bimodular Strength (MPa)
Sample1	1694.12	32.527	36.248	Sample16	1595.21	30.628	34.132
Sample2	1611.23	30.935	34.474	Sample17	1774.76	34.075	37.973
Sample3	1743.91	33.483	37.313	Sample18	1670.17	32.067	35.736
Sample4	1820.57	34.954	38.954	Sample19	1773.92	34.059	37.955
Sample5	1800.78	34.574	38.530	Sample20	1700.95	32.658	36.394
Sample6	1559.03	29.933	33.358	Sample21	1780.32	34.182	38.092
Sample7	1737.62	33.362	37.179	Sample22	1661.84	31.907	35.557
Sample8	1589.85	30.525	34.017	Sample23	1723.46	33.091	36.876
Sample9	1736.77	33.345	37.161	Sample24	1703.75	32.712	36.454
Sample10	1782.09	34.216	38.130	Sample25	1670.97	32.082	35.753
Sample11	1749.35	33.587	37.430	Sample26	1702.43	32.686	36.426
Sample12	1756.51	33.724	37.583	Sample27	1755.34	33.702	37.558
Sample13	1621.06	31.124	34.685	Sample28	1822.67	34.995	38.999
Sample14	1734.88	33.309	37.120	Sample29	1686.67	32.384	36.089
Sample15	1620.45	31.112	34.672	Sample30	1661.79	31.906	35.556

Unimodular and bimodular strength is calculated from the peak load obtained in four point bend test with 1/3 loading. The results of sixty small and thirty large specimens are tabulated in the Table 4.6 and Table 4.7.

(a) (b)

Fig. 4.11 Testing arrangement of flexural specimens having square cross-section applied to four-point bend with 1/3 loading (a) Large size and (b) Small size specimen

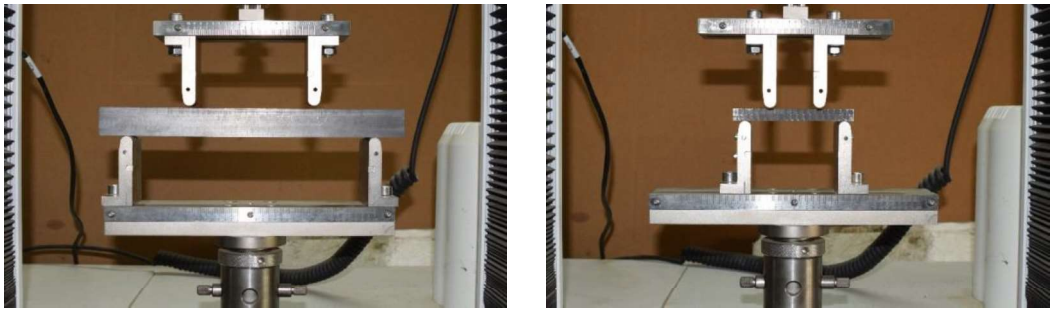

(a) (b)

Fig. 4.12 Testing arrangement of flexural specimens having square cross-section applied to four point bend with 1/4 loading (a) Large size and (b) Small size specimen

Table 4.6 Experimental test results for small specimen subjected to four-point bend test with 1/3 loading

Specimen No.	Peak load (N)	Unimodular Strength (MPa)	Bimodular Strength (MPa)	Specimen No.	Peak load (N)	Unimodular Strength (MPa)	Bimodular Strength (MPa)
Sample1	440.57	34.364	38.296	Sample31	438.49	34.20222	38.11531
Sample2	461.23	35.975	40.091	Sample32	478.45	37.3191	41.58879
Sample3	477.67	37.258	41.520	Sample33	486.12	37.91736	42.2555
Sample4	441.86	34.465	38.408	Sample34	501.58	39.12324	43.59934
Sample5	466.58	36.393	40.557	Sample35	470.67	36.71226	40.91252
Sample6	458.77	35.784	39.878	Sample36	449.17	35.03526	39.04365
Sample7	457.36	35.674	39.755	Sample37	505.92	39.46176	43.97659
Sample8	460.55	35.922	40.032	Sample38	494.22	38.54916	42.95958
Sample9	440.87	34.387	38.322	Sample39	481.64	37.56792	41.86608
Sample10	479.48	37.399	41.678	Sample40	429.98	33.53844	37.37558
Sample11	471.12	36.747	40.951	Sample41	491.96	38.37288	42.76313
Sample12	465.55	36.312	40.467	Sample42	487.24	38.00472	42.35285
Sample13	409.95	31.976	35.634	Sample43	481.78	37.57884	41.87825
Sample14	460.86	35.947	40.059	Sample44	456.67	35.62026	39.69558
Sample15	424.22	33.089	36.874	Sample45	488.75	38.1225	42.48411
Sample16	468.75	36.562	40.745	Sample46	474.89	37.04142	41.27934
Sample17	469.78	36.642	40.835	Sample47	485.79	37.89162	42.22681
Sample18	472.78	36.876	41.095	Sample48	489.96	38.21688	42.58928
Sample19	441.78	34.458	38.401	Sample49	440.76	34.37928	38.31262
Sample20	472.84	36.881	41.101	Sample50	489.01	38.14278	42.50671
Sample21	470.29	36.682	40.879	Sample51	493.05	38.4579	42.85788
Sample22	486.76	37.967	42.311	Sample52	480.74	37.49772	41.78784
Sample23	430.48	33.577	37.419	Sample53	487.98	38.06244	42.41717
Sample24	460.97	35.955	40.069	Sample54	501.25	39.0975	43.57066
Sample25	470.25	36.679	40.876	Sample55	492.59	38.42202	42.81789
Sample26	470.05	36.663	40.858	Sample56	473.67	36.94626	41.17329
Sample27	449.89	35.091	39.106	Sample57	496.95	38.7621	43.19688
Sample28	462.44	36.070	40.197	Sample58	479.41	37.39398	41.67224
Sample29	490.54	38.262	42.639	Sample59	466.67	36.40026	40.56482
Sample30	480.17	37.453	41.738	Sample60	495.34	38.63652	43.05694

Table 4.7 Experimental test results for large specimen subjected to four-point bend test with 1/3 loading

Specimen No.	Peak load	Unimodular Strength (Mpa)	Bimodular Strength (Mpa)	Specimen No.	Peak load	Unimodular Strength (Mpa)	Bimodular Strength (Mpa)
Sample1	2590.21	32.325	36.024	Sample16	2602.54	32.479	36.195
Sample2	2637.08	32.91	36.676	Sample17	2736.89	34.156	38.062
Sample3	2490.54	31.081	34.638	Sample18	2540.31	31.703	35.33
Sample4	2638.15	32.924	36.69	Sample19	2771.23	34.584	38.541
Sample5	2456.45	30.656	34.163	Sample20	2638.94	32.933	36.701
Sample6	2577.04	32.161	35.841	Sample21	2762.45	34.475	38.419
Sample7	2773.64	34.615	38.575	Sample22	2860.88	35.703	39.788
Sample8	2829.74	35.315	39.355	Sample23	2835.22	35.383	39.431
Sample9	2565.54	32.017	35.681	Sample24	2775.08	34.633	38.595
Sample10	2727.75	34.042	37.937	Sample25	2702.98	33.733	37.592
Sample11	2854.34	35.622	39.697	Sample26	2734.42	34.125	38.029
Sample12	2719.53	33.939	37.822	Sample27	2580.19	32.2	35.884
Sample13	2510.47	31.33	34.915	Sample28	2714.23	33.873	37.749
Sample14	2763.32	34.486	38.431	Sample29	2677.72	33.417	37.241
Sample15	2699.54	33.69	37.544	Sample30	2625.36	32.764	36.513

Fig. 4.12(a) elucidates arrangement of flexural testing for four point with 1/4 loading for large specimen whereas Fig. 4.12(b) describes the same for small flexural specimen. The unimodular and bimodular strengths are calculated from peak load obtained in four point bend test with 1/4 loading using following expression:

$$\sigma_{u4pbt1/4} = \left(\frac{3PL_0}{4bd^2}\right) \qquad \text{(Unimodular strength)} \qquad (4.44)$$

$$\sigma_{b4pbt1/4} = \left(\frac{3PL_0(1+\sqrt{\alpha})}{8bd^2}\right) \qquad \text{(Bimodular strength)} \qquad (4.45)$$

Table 4.8 Experimental test results for small four-point bend specimens with ¼ loading

Specimen No.	Peak load(N)	Unimodular Strength (Mpa)	Bimodular Strength (Mpa)	Specimen No.	Peak load(N)	Unimodular Strength (Mpa)	Bimodular Strength (Mpa)
Sample1	600.65	36.039	40.162	Sample31	620.29	37.217	41.475
Sample2	601.49	36.089	40.218	Sample32	613.87	36.832	41.046
Sample3	616.56	36.993	41.226	Sample33	629.21	37.752	42.071
Sample4	628.09	37.685	41.997	Sample34	633.54	38.012	42.361
Sample5	619.28	37.156	41.407	Sample35	640.57	38.434	42.831
Sample6	624.45	37.467	41.753	Sample36	596.95	35.817	39.914
Sample7	625.39	37.523	41.816	Sample37	643.66	38.619	43.038
Sample8	668.14	40.088	44.674	Sample38	645.85	38.751	43.184
Sample9	542.54	32.552	36.276	Sample39	634.67	38.080	42.436
Sample10	607.76	36.465	40.637	Sample40	583.42	35.005	39.010
Sample11	647.16	38.829	43.272	Sample41	614.53	36.871	41.090
Sample12	645.02	38.701	43.129	Sample42	631.65	37.899	42.235
Sample13	549.72	32.983	36.756	Sample43	645.94	38.7564	43.190
Sample14	634.78	38.086	42.444	Sample44	632.93	37.9758	42.320
Sample15	602.91	36.174	40.313	Sample45	670.57	40.2342	44.837
Sample16	608.12	36.487	40.661	Sample46	644.78	38.6868	43.112
Sample17	637.69	38.261	42.638	Sample47	633.86	38.0316	42.382
Sample18	667.39	40.043	44.624	Sample48	598.45	35.907	40.015
Sample19	573.32	34.399	38.334	Sample49	612.75	36.765	40.971
Sample20	632.13	37.927	42.267	Sample50	622.39	37.3434	41.615
Sample21	632.56	37.953	42.295	Sample51	584.56	35.0736	39.086
Sample22	648.46	38.907	43.359	Sample52	626.94	37.6164	41.920
Sample23	636.66	38.199	42.570	Sample53	628.27	37.6962	42.009
Sample24	593.65	35.619	39.694	Sample54	630.53	37.831	42.160
Sample25	610.57	36.634	40.825	Sample55	641.38	38.4828	42.885
Sample26	645.55	38.733	43.164	Sample56	635.76	38.1456	42.509
Sample27	643.78	38.626	43.046	Sample57	627.32	37.6392	41.945
Sample28	626.37	37.582	41.881	Sample58	624.14	37.448	41.732
Sample29	572.42	34.345	38.274	Sample59	621.35	37.281	41.546
Sample30	610.87	36.652	40.845	Sample60	590.56	35.433	39.487

The unimodular and bimodular strength is calculated from the peak load obtained in four point bend test with 1/4 loading. The results obtained from these tests for small and large specimens are tabulated in the Table 4.8 and Table 4.9.

Table 4.9 Experimental test results for large four-point bend specimens with ¼ loading

Specimen No.	Peak load	Unimodular Strength (Mpa)	Bimodular Strength (Mpa)	Specimen No.	Peak load	Unimodular Strength (Mpa)	Bimodular Strength (Mpa)
Sample1	3411.54	32.750	36.497	Sample16	3725.18	35.76173	39.85324
Sample2	3509.76	33.693	37.548	Sample17	3646.05	35.00208	39.00668
Sample3	3512.64	33.721	37.579	Sample18	3451.96	33.13882	36.93024
Sample4	3753.62	36.034	40.157	Sample19	3340.76	32.0713	35.74058
Sample5	3455.56	33.173	36.968	Sample20	3605.23	34.61021	38.56997
Sample6	3651.17	35.051	39.061	Sample21	3508.64	33.68294	37.53662
Sample7	3606.54	34.622	38.583	Sample22	3626.56	34.81498	38.79817
Sample8	3511.32	33.708	37.565	Sample23	3618.44	34.73702	38.7113
Sample9	3766.95	36.162	40.300	Sample24	3458.76	33.2041	37.00299
Sample10	3637.27	34.917	38.912	Sample25	3617.13	34.72445	38.69728
Sample11	3078.45	29.553	32.934	Sample26	3489.04	33.49478	37.32693
Sample12	3648.76	35.028	39.035	Sample27	3345.74	32.1191	35.79386
Sample13	3653.98	35.078	39.091	Sample28	3659.29	35.12918	39.14832
Sample14	3698.33	35.503	39.565	Sample29	3353.43	32.19293	35.87613
Sample15	3435.22	32.978	36.751	Sample30	3445.46	33.07642	36.8607

4.4.1 Estimation of Weibull Parameters

Designing the structural components fabricated from ceramic materials like nuclear graphite requires its ability to explore failure statistics from appropriate numbers of test specimens to the real components, which then must be accounted

for strength-size-scaling (Quinn and Morrell 1991; Quinn 2003b, a; Bhushan et al. 2016). The probability of failure of components for the unimodular and bimodular stress field has been evaluated from the Weibull effective volume and area of the flexural beam with different size and applied loading conditions. In this manuscript; the analytical formulation are developed for finding the effective volume and effective surface area in the bimodular stress field for the rectangular cross-sectioned beam. To evaluate the effective volume and effective surface area and to deal with the probability of failure for a component at room temperature using appropriate ASTM standards, the component or test specimen should be treated as a system. This typical approach to design the structural components with varying complex stress fields requires discretizing the component in order to characterize the stress field using finite element (FE) solution. As the component failure might initiate in any of the discrete elements considered to be the weakest link, it is appropriate to consider a component as a system and utilize system reliability theories. Based on the weakest link theory, the component is considered to be a series system consisting of a chain or link of elements. Failure in one discrete element leads to a sudden catastrophic failure of the whole component. Accordingly, one needs a distribution that describes this extreme phenomenon of the sudden failure of the whole component due to the failure of a small weakest link (element)(Peirce 1926). The Weibull distribution with the weakest-link system approach is well-known as Weibull theory (Weibull 1939b, 1951). The Weibull plot depicting the probability of failure for three point and four point bend specimens for two loading conditions, namely flexural 1/3 loading and flexural 1/4 loading condition have been shown in Fig. 4.13 to 4.18 with the aid of best possible fit line using Linear regression (LIN2), Biased Maximum Likelihood

Estimator (MLE2-B) and Unbiased Maximum Likelihood Estimator (MLE2-U) for small and large size specimen using Weibpar (Weibull Distribution Parameter Estimation) version-4.3 and CARES (Ceramics Analysis and Reliability Evaluation of Structures) version-9.3.2.196 Software developed by Connecticut Reserve Technologies, (NASA) USA.

Weibull plot for all different flexural conditions has been plotted from the experimental data based on the concepts of weakest link theory(Duffy et al. 1992). The strength dependancy on size has been assessed from the Weibull probability of failure plot (Figs. 4.13-4.18) for characterizing the unimodular and bimodular strength of the three-point and four-point flexural specimens with 1/3 and ¼ loading conditions. For every flexural small and large loading condition, small and large squared cross-sectioned beams have been analyzed for quantifying the size effect. Each of Figs. 4.13-4.18 consists of four parts, typically (a) & (b) refers to the unimodular strength, (c) & (d) concerns with the bimodular strength. The Figures part (a) and (c) of the probability plot shows a graph with observed fractured strength (unimodular and bimodular) on horizontal axis and cumulative probability of failure on vertical axis. The Weibull probability plot is used to test whether or not a dataset follows Weibull distribution. The abscissa and ordinate of the distribution plot are scales of type Log_e and Double Log_e Reciprocal respectively. If all the scatter points are close to the reference line, we can say that the dataset follows the Weibull distribution. The horizontal axis is expanded within the range limit of peak load found from experiments for better interpretation of the plot. The Illustrations of part (b) and (d) (concerns with the unimodular and bimodular strength respectively) represents the histogram plot

between the frequency (probability density function) on vertical axis and flexural strength of test specimens on horizontal axis. These plots show the Weibull distribution with least square estimator, maximum likelihood estimator biased, maximum likelihood estimator unbiased and compared with normal distribution. The random flexural strength data is plotted in the square bar chart form and it is clearly visible that normal distribution is not able to fit the failure data set.

Stochastic tools Linear regression (LIN2), biased maximum likelihood estimator (MLE2-B) and unbiased maximum likelihood estimator (MLE2-U) have been employed for determining the best fit line of the Weibull distribution of the failure data set. The probability of failure of component has been evaluated as a function of fracture strength using Weibull statistical model. The sufficiency of failure strength data set is a necessaity for the appropriateness and reliability of Weibull model, although it puts a constraint in terms of cost of experimentation. Therefore, the experimental testing is carried out successfully for one hundred seventy-eight small and ninety large specimens in different flexural conditions to justify the Weibull statistical model. The reduced number of large specimens can be ascribed to their high cost in comparison to small specimens. The three sets of large flexural and three sets of small flexural specimen test data are taken to characterize the size effect on fracture strength. Stochastic analysis of these randomly distributed data has been carried out to characterize the graphite component failure. In the flexural specimens, there are two different strength obtained from single test apropos as (i) unimodular classical strength (obtained from Eqs. 4.40, 4.42 and 4.44) and (ii) bimodular strength (obtained from Eqs. 4.41, 4.43 and 4.45) and understandably these values are significantly different for the graphite material tested in lab. The success of fitting the Weibull distribution

through the normalized data sets allows us to improve the basis for the estimates of the variability. This could also imply that the variability on the graphite strength for the different strength measures is based on the same flaw distribution and thus a property of the material.

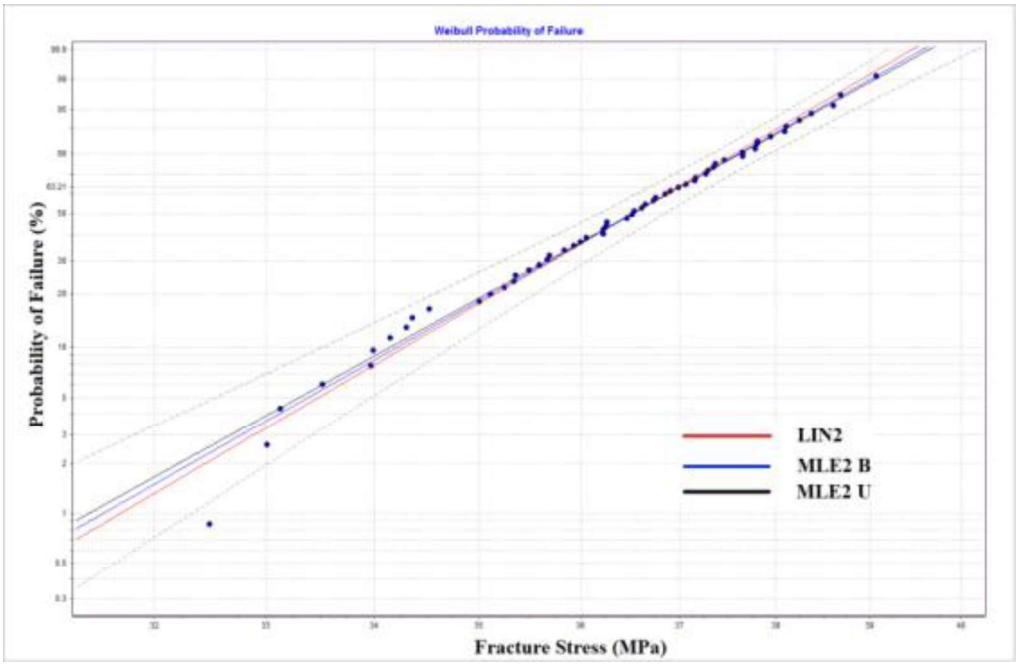

(a)

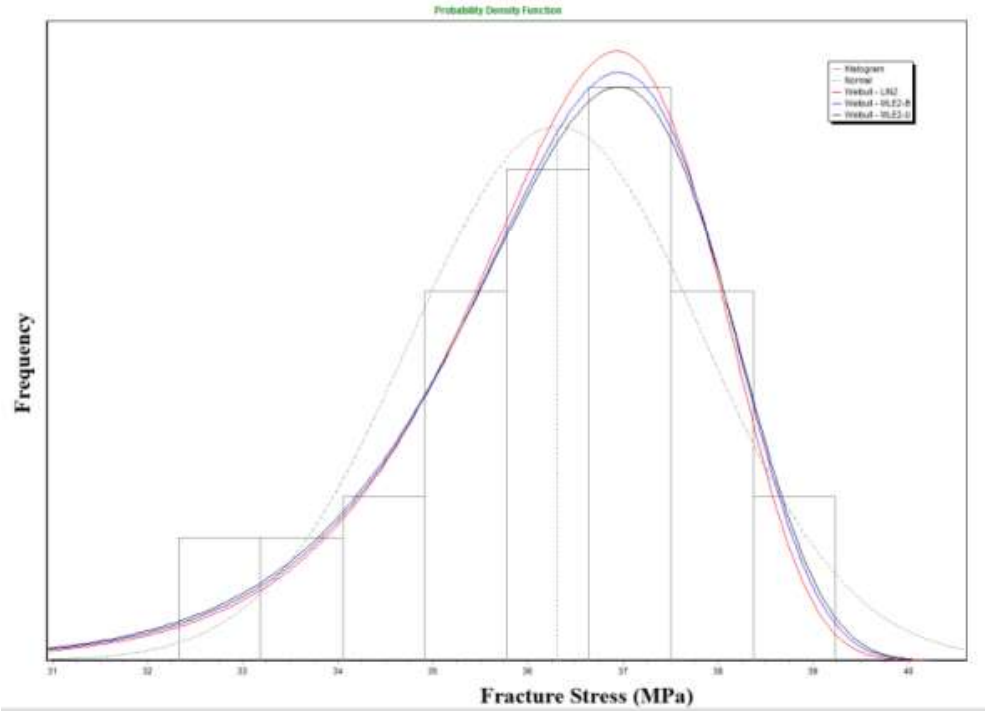

(b)

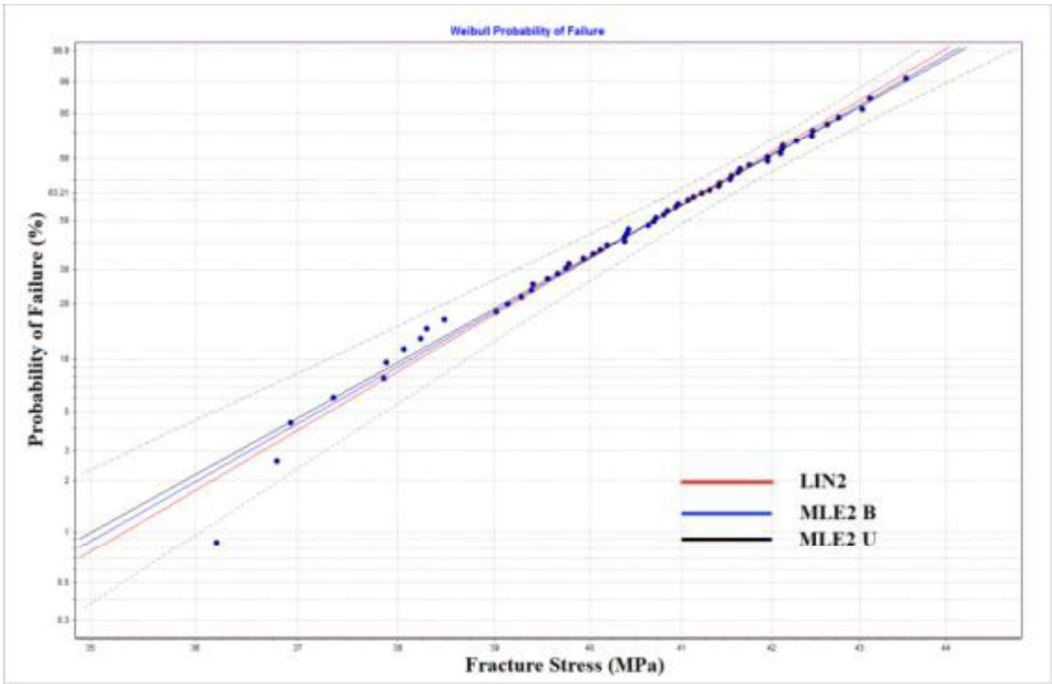

(c)

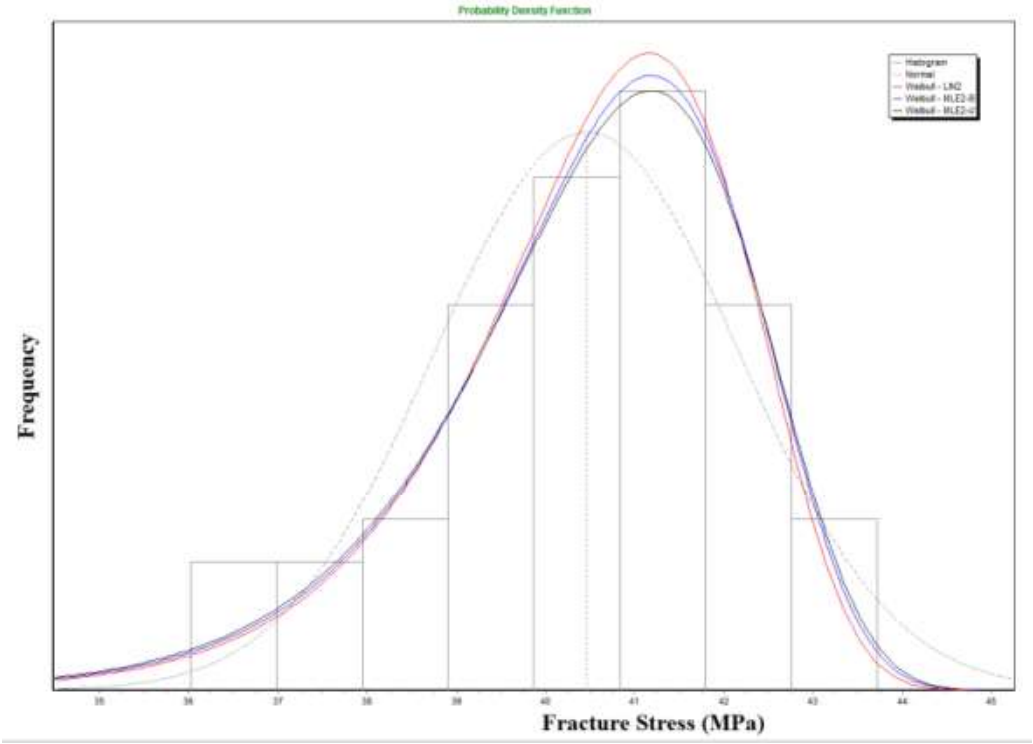

(d)

Fig.4.13. Weibull probability plot for small three point bend specimen best fit line for LIN2 (Linear regression with two parameter Weibull distribution), MLE2-B (Biased maximum likelihood estimator with two parameter Weibull distribution)

and MLE2-U (Unbiased maximum likelihood estimator with two parameter Weibull distribution parameter Weibull distribution) (b) Weibull PDF and Normal PDF plot and the failure strength data plot in histogram form for unimodular strength characterization. (c) Weibull plot and (d) Histogram plot for bimodular strength characterization

Presence of flaws, defects and their random distribution/clustering or orientation over volume and area requires fracture strength to be quantified particularly for high risk components, which nevertheless is to qualify as a material property for component design.

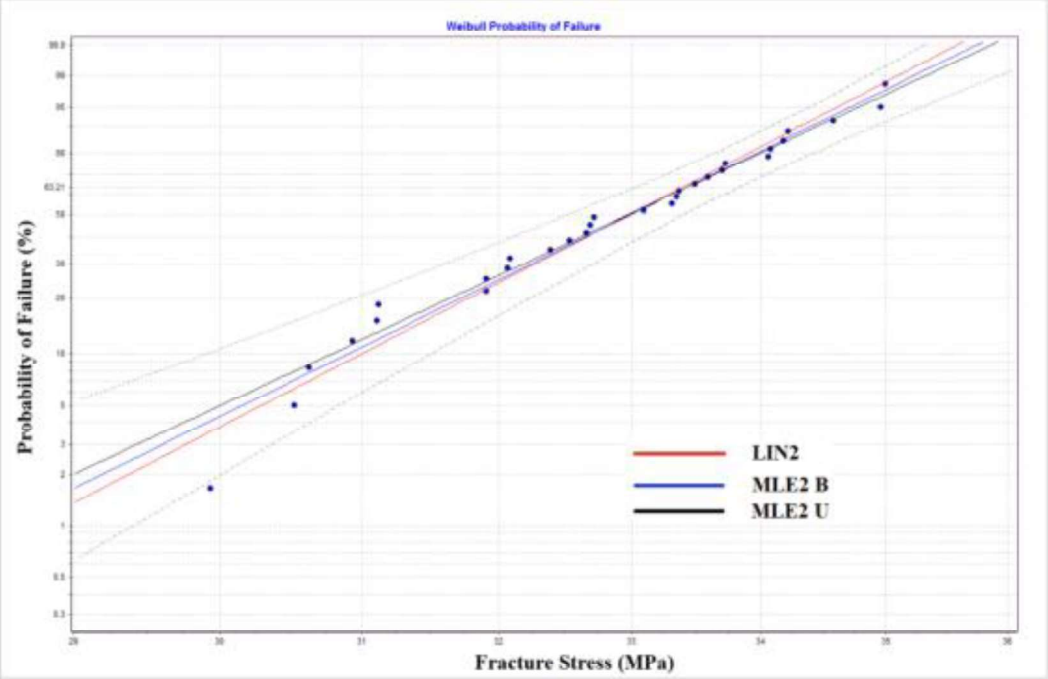

(a)

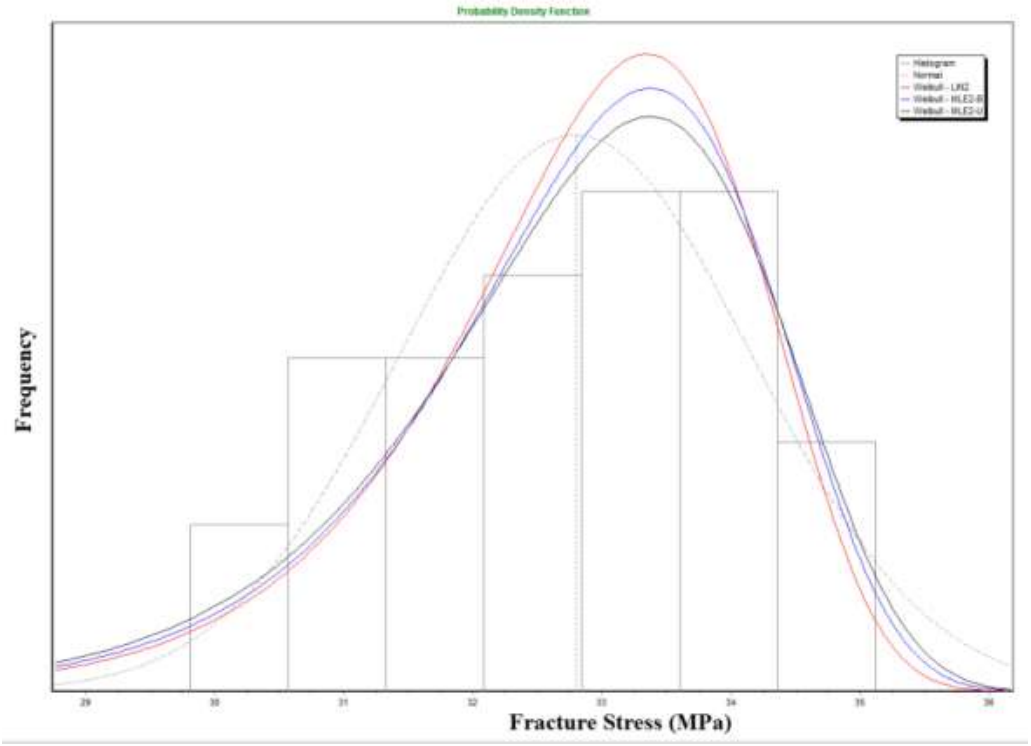
Probability Density Function
Frequency
Fracture Stress (MPa)

(b)

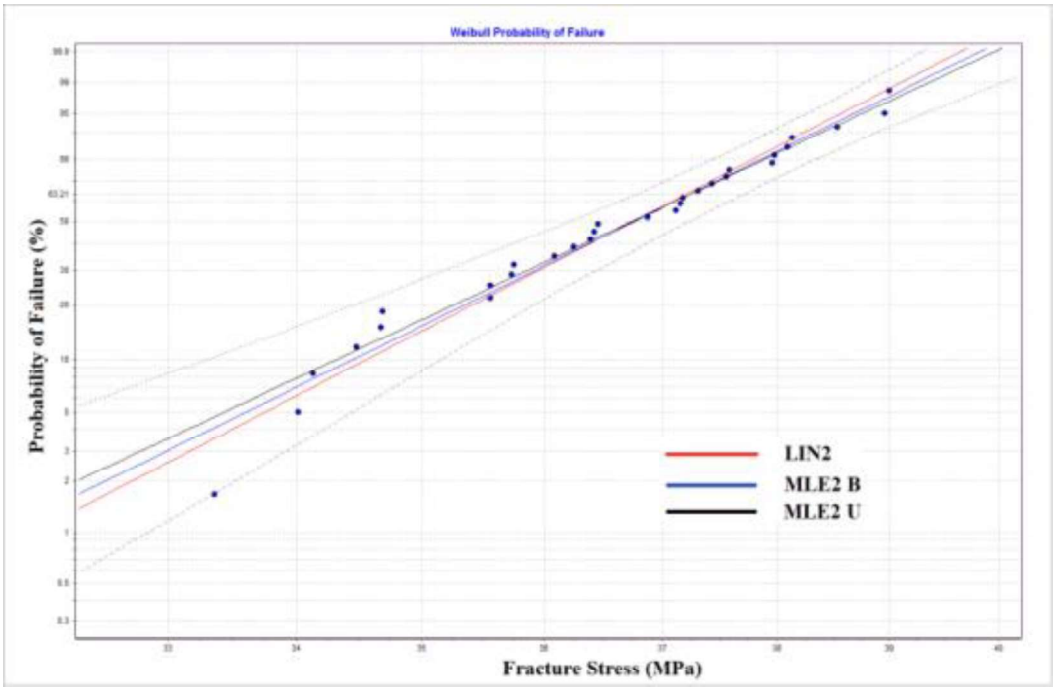
Weibull Probability of Failure
Probability of Failure (%)
Fracture Stress (MPa)
LIN2
MLE2 B
MLE2 U

(c)

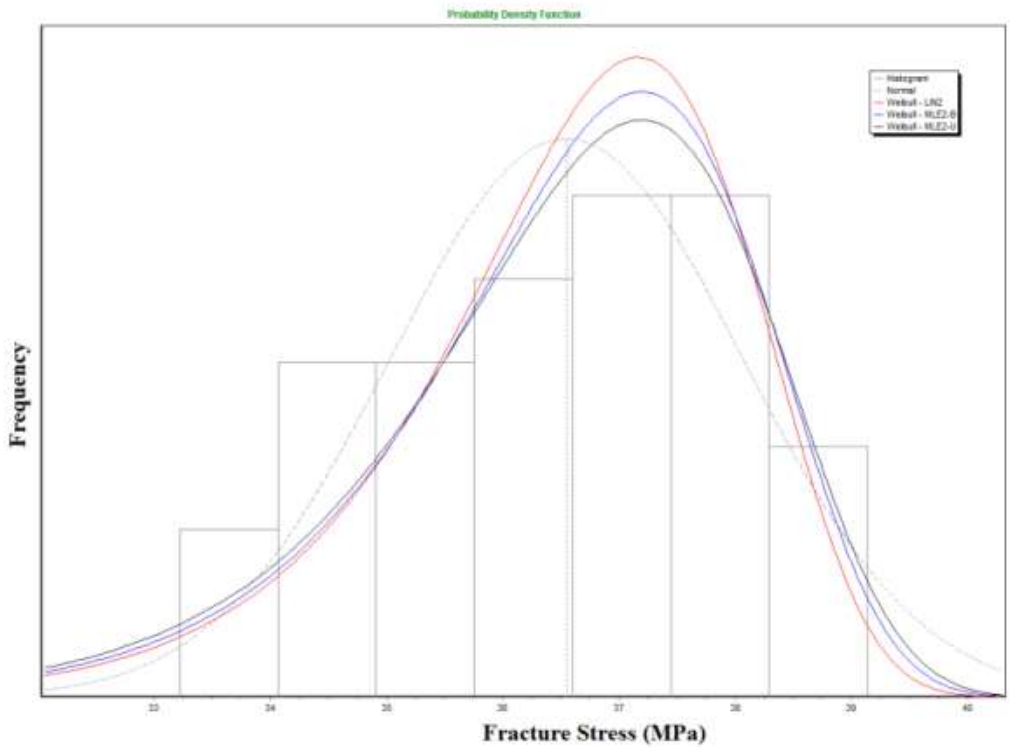

(d)

Fig. 4.14. (a) Weibull probability of failure plot with best fit line for LIN2, MLE2-B, and MLE2-U (b) Weibull PDF and Normal PDF plot and the failure strength data plot in histogram form for unimodular and (c) Weibull probability plot, (d) Histogram plot for Bimodular strength characterization for large three-point bend specimen.

As the real components and lab specimens vary in size, experimental values need to be extrapolated for a reliable design and life prediction of the graphite component part. Therefore, a unique tensile strength value has to be predicted first for the material for size dependence strength prediction. This has been determined from the probability of failure versus unimodular and bimodular flexural strength distribution plot of the Weibull model of experimental data sets (refer Figs 4.15 to 4.19).

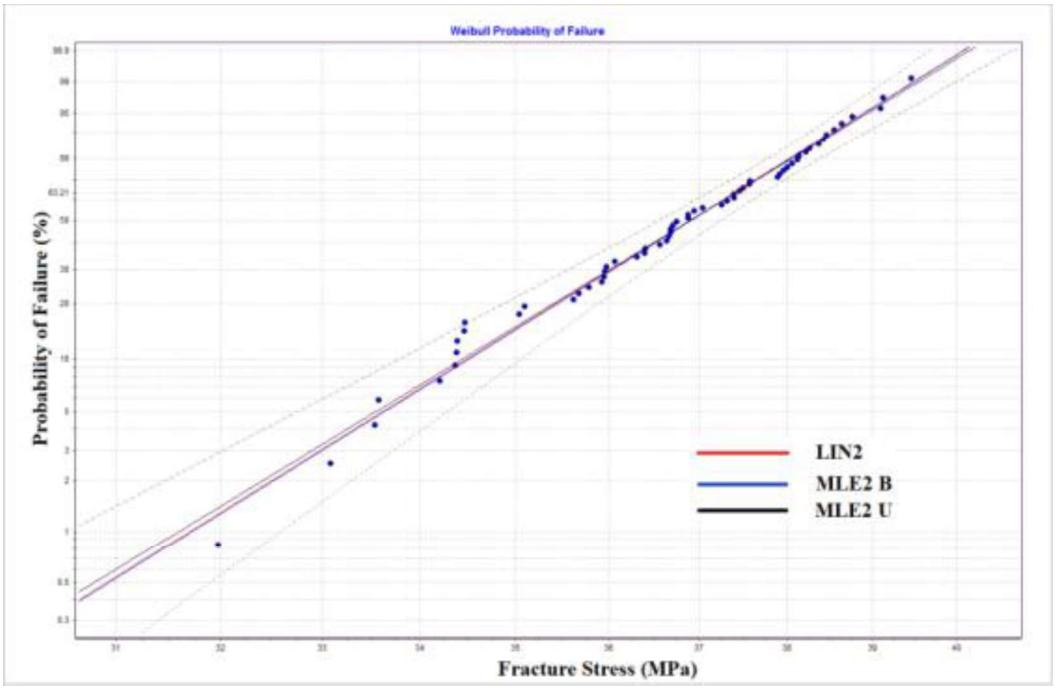
Weibull Probability of Failure
Probability of Failure (%)
Fracture Stress (MPa)
LIN2
MLE2 B
MLE2 U

(a)

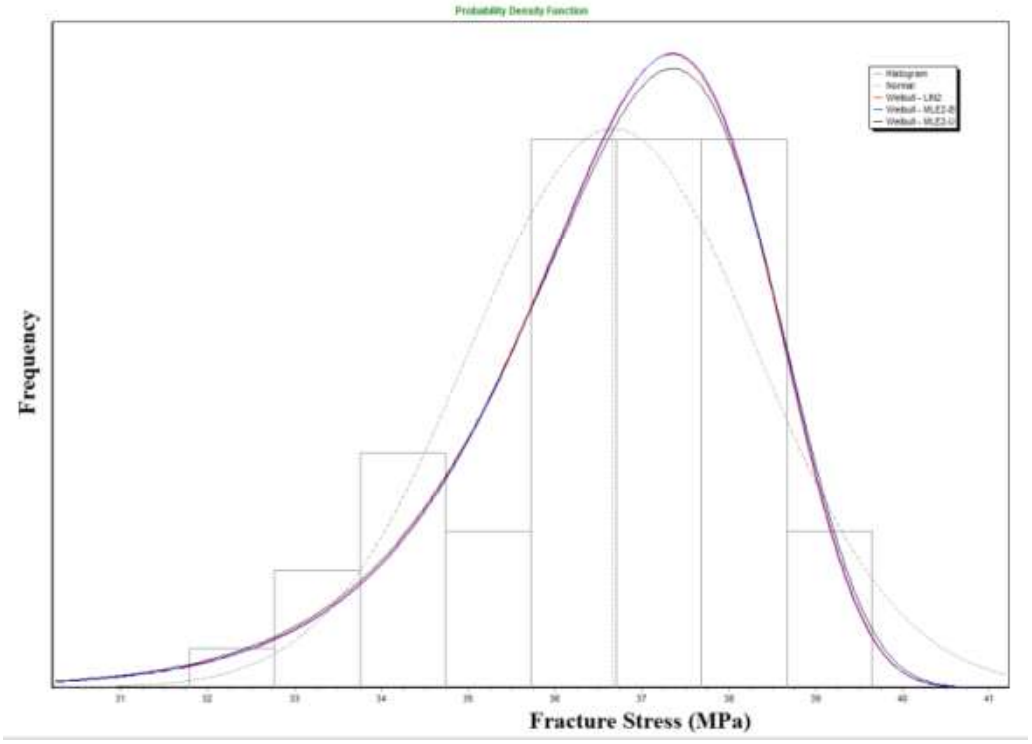
Probability Density Function
Frequency
Fracture Stress (MPa)

(b)

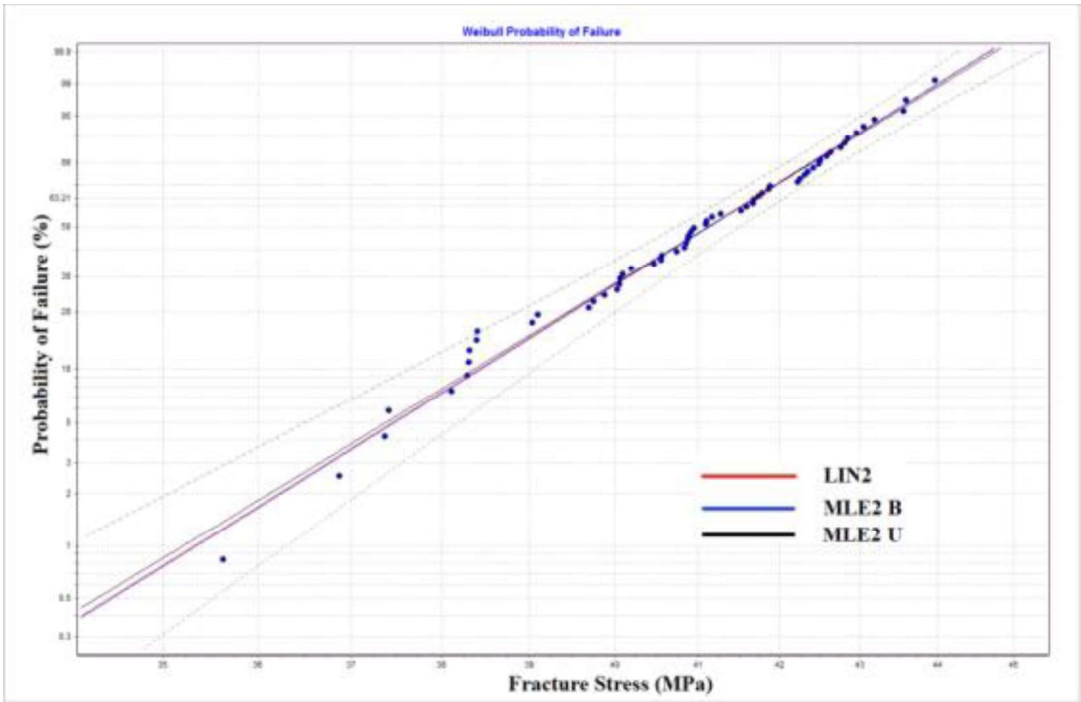

(c)

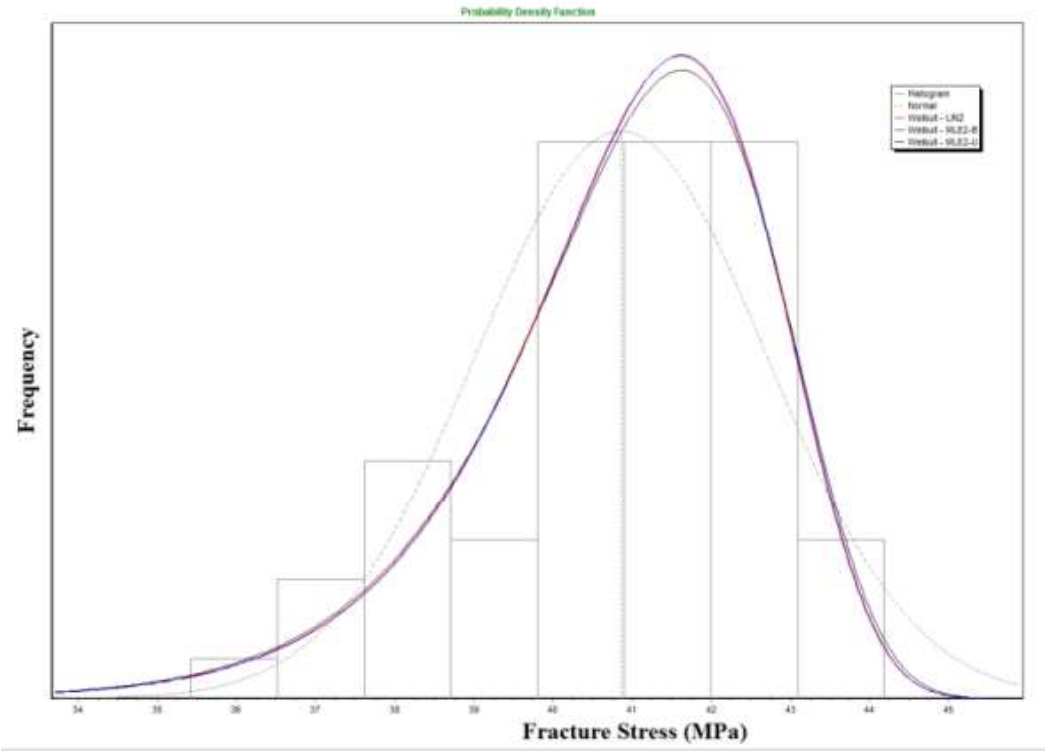

(d)

Fig. 4.15. (a) Weibull probability of failure plot with best fit line for LIN2, MLE2-B, and MLE2-U (b) Weibull PDF and Normal PDF plot and the failure

strength data plot in histogram form for unimodular and (c) Weibull probability plot, (d) Histogram plot for Bimodular strength characterization for small four point flexural 1/3 loading specimen.

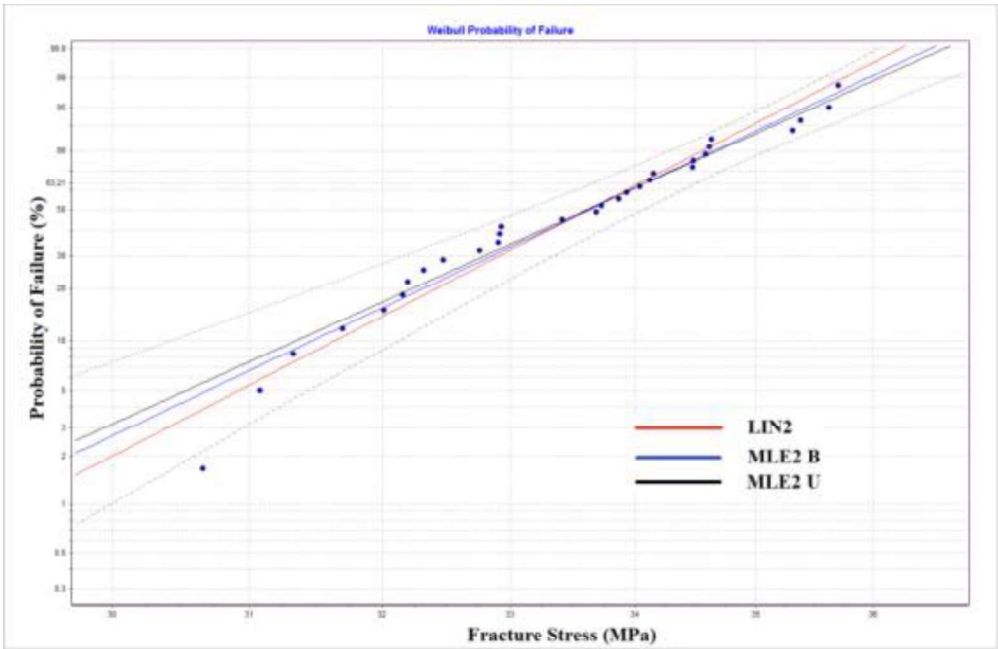

(a)

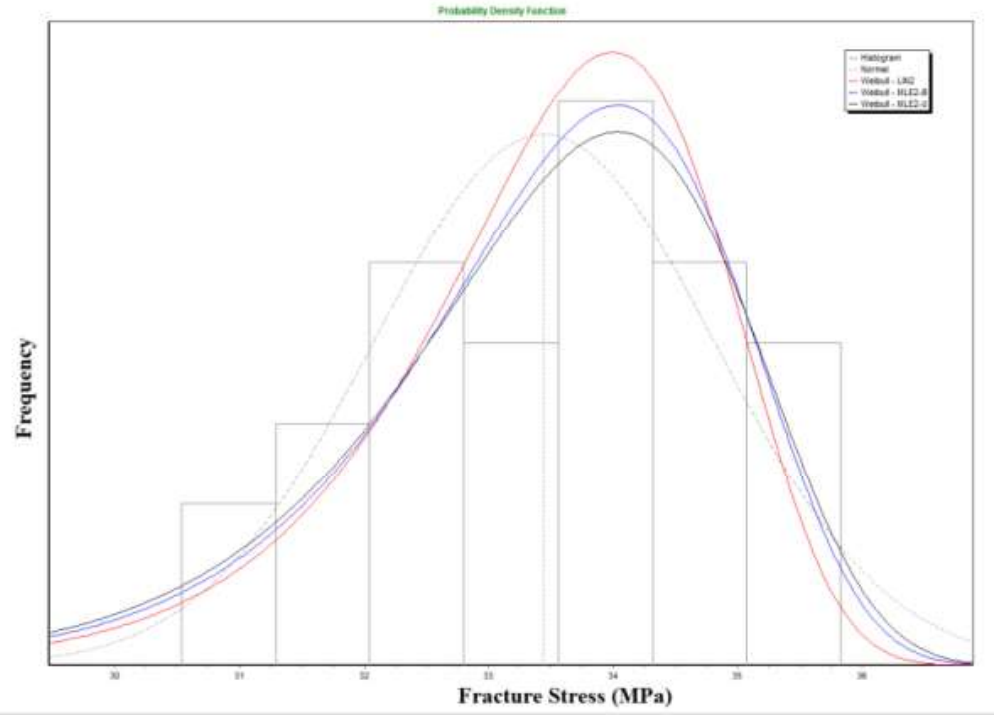

(b)

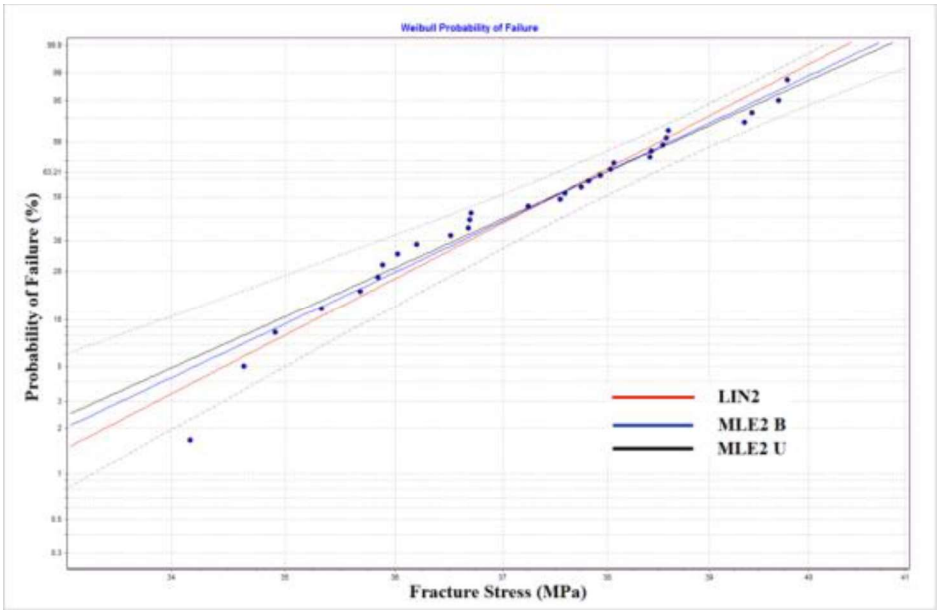

(c)

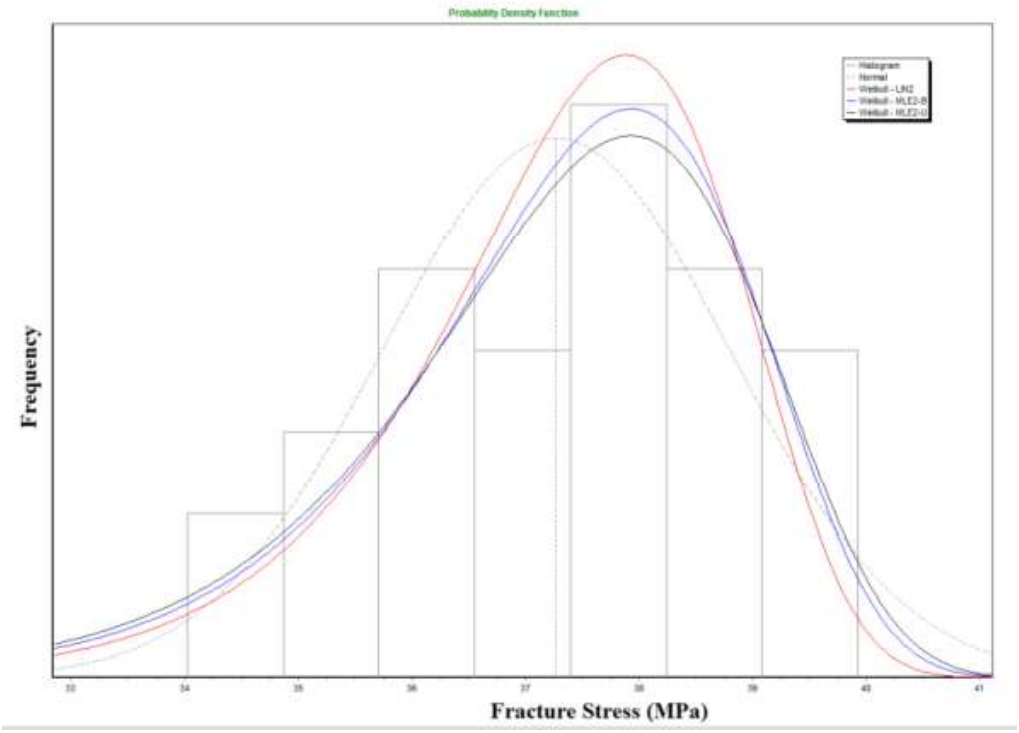

(d)

Fig. 4.16. (a) Weibull probability of failure plot with best fit line for LIN2, MLE2-B, and MLE2-U (b) Weibull PDF and Normal PDF plot and the failure strength data plot in histogram form for unimodular and (c) Weibull probability

plot, (d) Histogram plot for Bimodular strength characterization for large four point flexural 1/3 loading specimen.

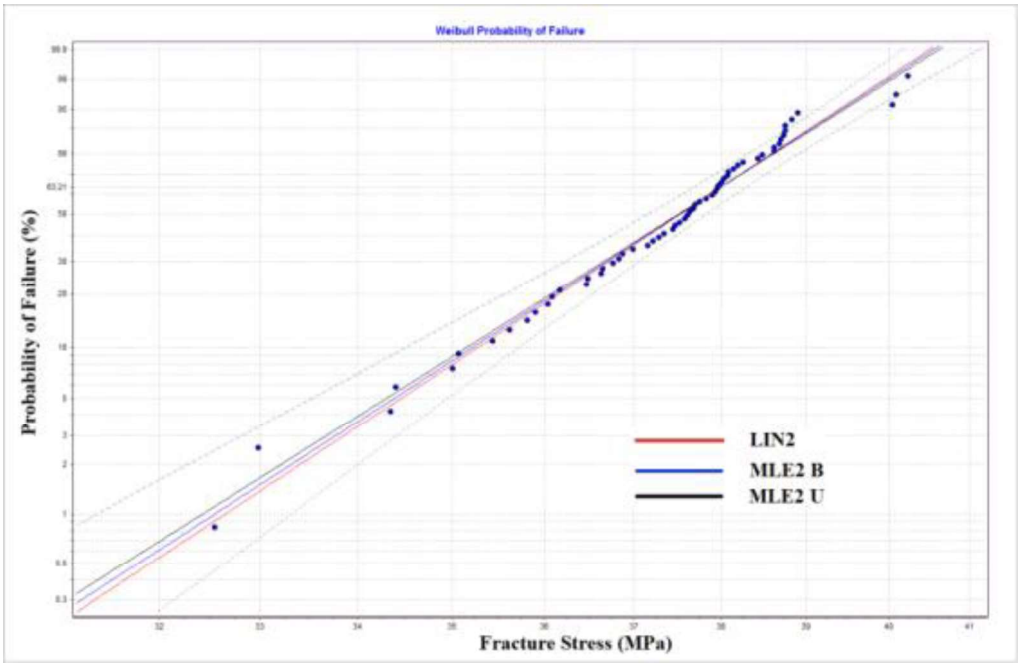

(a)

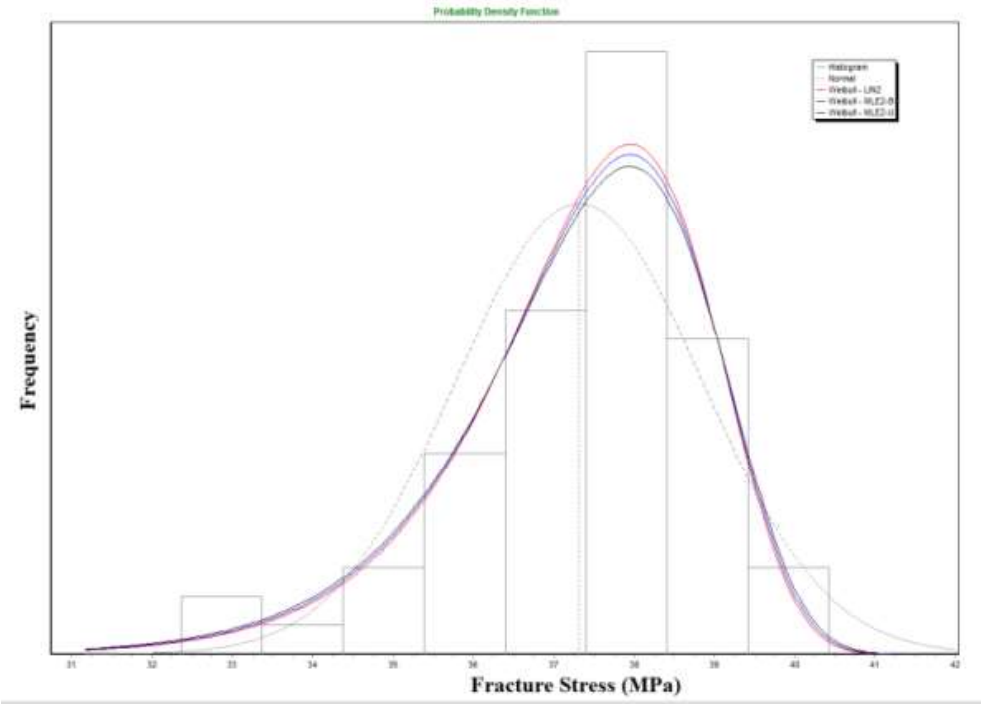

(b)

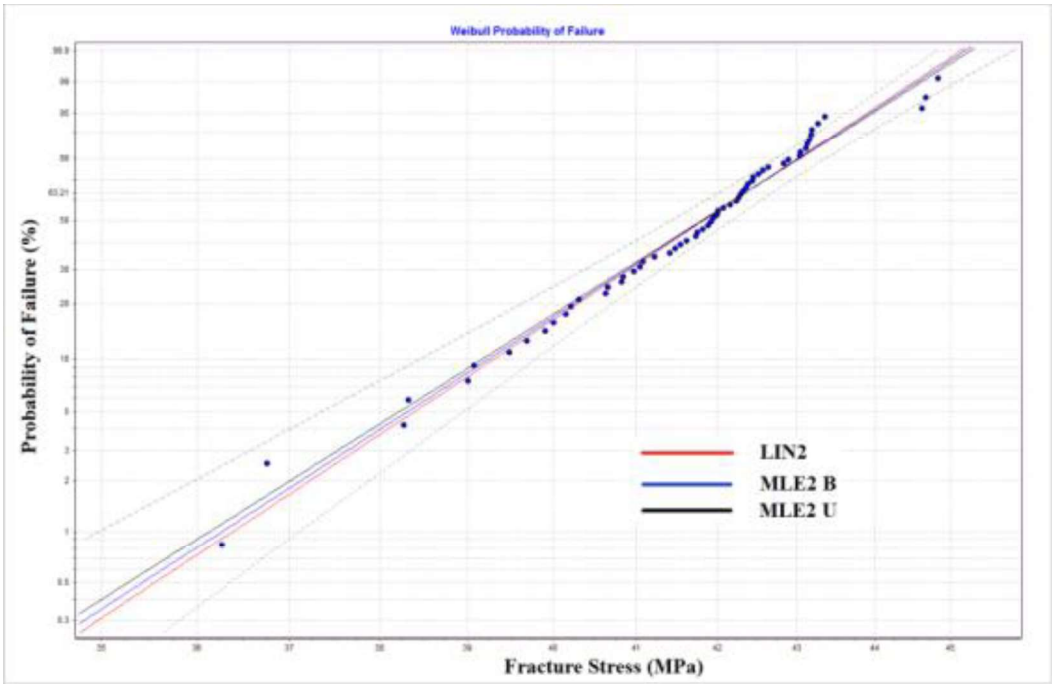

(c)

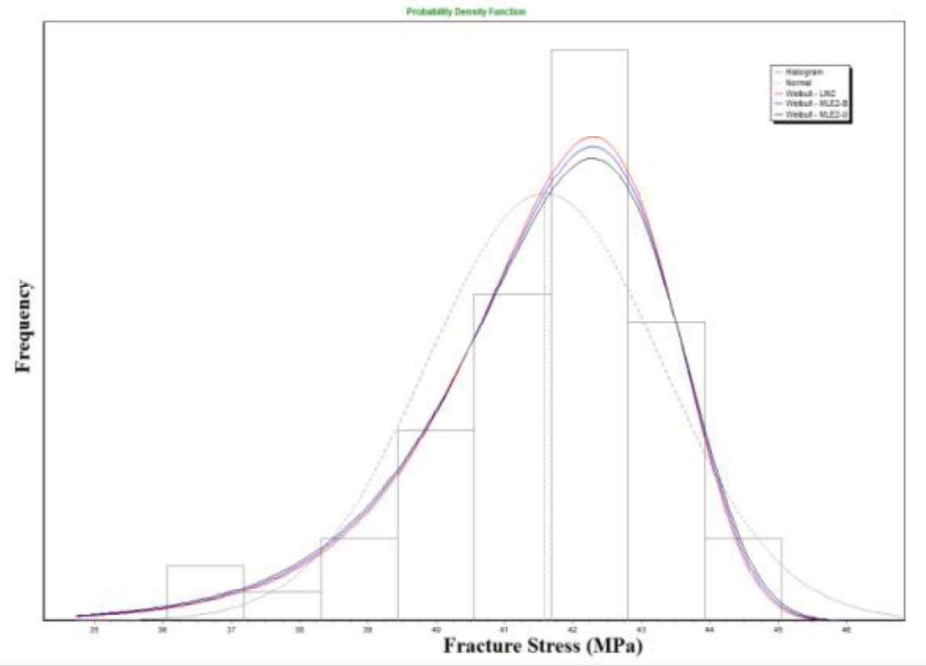

(d)

Fig. 4.17. (a) Weibull probability of failure plot with best fit line for LIN2, MLE2-B, and MLE2-U (b) Weibull PDF and Normal PDF plot and the failure strength data plot in histogram form for unimodular and (c) Weibull probability

plot, (d) Histogram plot for Bimodular strength characterization for small four point flexural 1/4 loading specimen.

As the size of a component or test specimen geometry is increased, then, on an average, the tensile strength of the component decreases. The reason for this is that as the volume (or surface area) of the component is increased, the likelihood of encountering a critical flaw with deleterious orientations to the load applied increases.

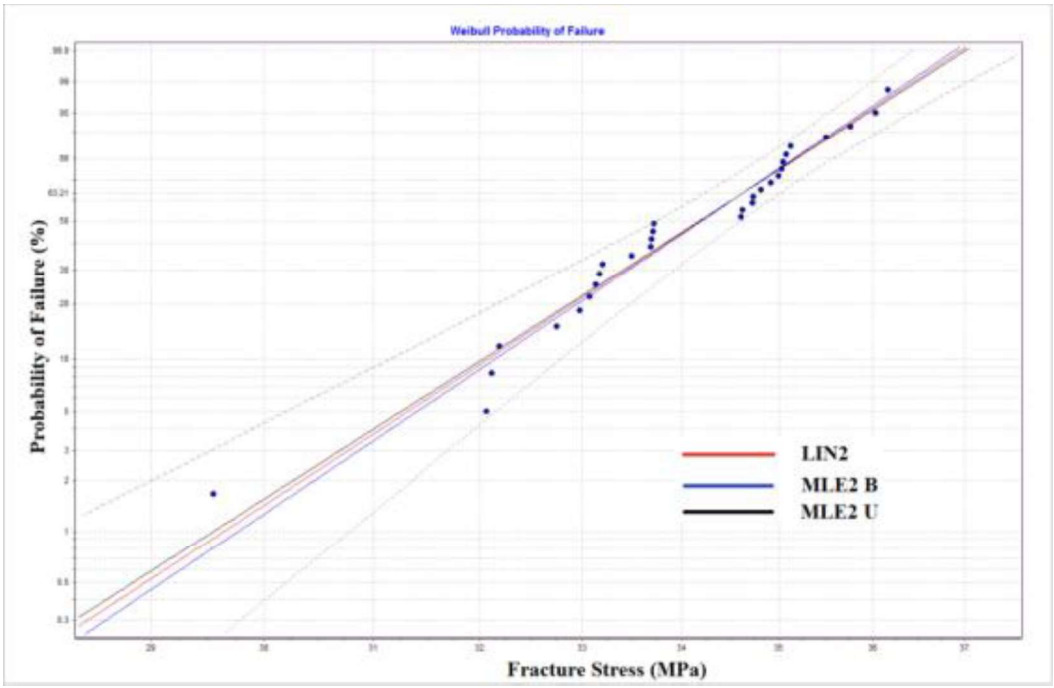

(a)

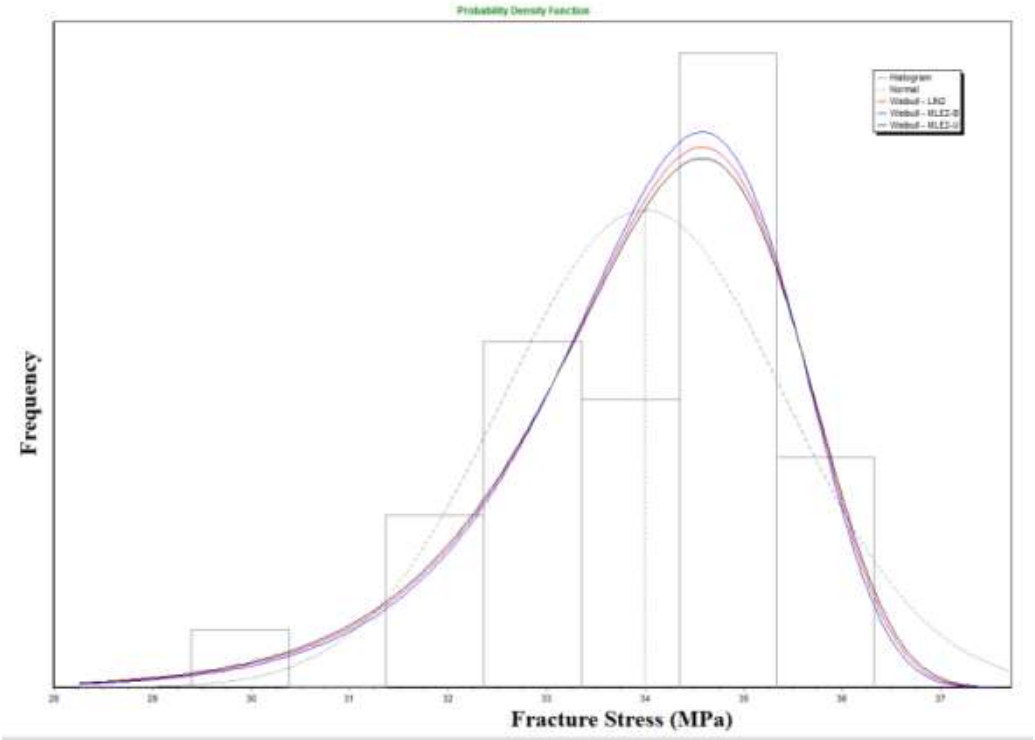
Probability Density Function
Frequency
Fracture Stress (MPa)

(b)

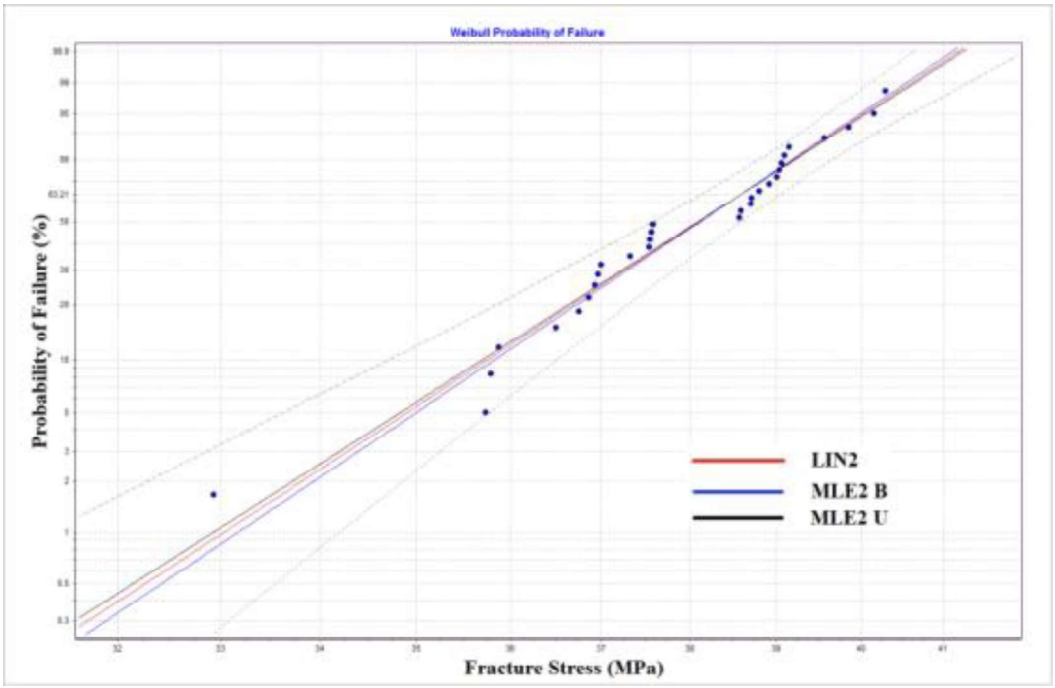
Weibull Probability of Failure
Probability of Failure (%)
Fracture Stress (MPa)
LIN2
MLE2 B
MLE2 U

(c)

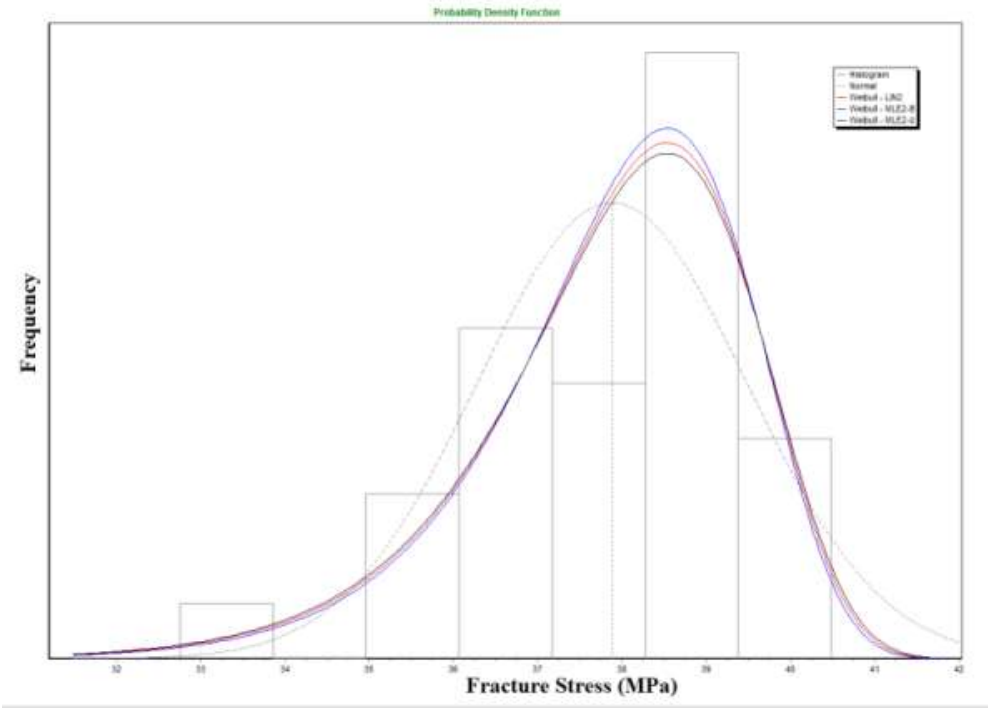

(d)

Fig. 4.18. (a) Weibull probability of failure plot with best fit line for LIN2, MLE2-B, and MLE2-U (b) Weibull PDF and Normal PDF plot and the failure strength data plot in histogram form for unimodular and (c) Weibull probability plot, (d) Histogram plot for Bimodular strength characterization for large four point flexural 1/4 loading specimen.

Therefore, to estimate the unique flexural strength for this material, Weibull distribution plot for cumulative probability of failure has been plotted against the flexural strength. With reference to Figs. Part (a) and (c) of the Weibull plot, the cumulative probability of failure is obtained by the following ranking scheme as per ASTM C 1239 (ASTM C1239 −13 2013).

$$P_i = \frac{i - 0.5}{n} \tag{4.46}$$

where P_i is the ranked cumulative probability, i is the rank of the individual specimen arranged in increasing order of tensile strength and n is the total number

of specimens tested. The probability of failure against tensile strength data set has been plotted with 90% confidence bound for all the three estimator**.** The scattered data on the Weibull plot has been analyzed using the best fit line drawn by least square estimator (LIN2), biased (MLE2-B) and unbiased (MLE2-U) maximum likelihood estimator procedure.

Linear regression using least square estimator requires the application of a ranking rule for all the failure load data to estimate the failure probability of each data. Once an estimate of individual probabilities is made, the failure data is regressed to determine the distribution parameters. Finding distribution parameters via linear regression involves utilizing the ranked probability of failure along with the associated failure stresses in the following expression based on Weibull weakest link theory (Weibull 1939b, 1951).

$$P_i = 1 - \exp\left[-\left\{ \frac{\sigma}{\sigma_\theta} \right\}^m \right] \qquad \sigma > 0 \qquad (4.47)$$

$$P_i = 0 \qquad \sigma \le 0 \qquad (4.48)$$

Where, P_i is probability of failure, σ is flexural strength (maximum stress obtain from experiment) attained during experiment, σ_θ is Weibull scale parameter or characteristic strength at 63.21% of probability of failure and *m* is shape parameter or Weibull modulus. The derivative of Eqs (4.47) and (4.48) gives the expression for the probability density function and is written as:

$$f(\sigma) = \left\{ \frac{m}{\sigma_\theta} \right\} \left\{ \frac{\sigma}{\sigma_\theta} \right\}^{m-1} \exp\left[-\left\{ \frac{\sigma}{\sigma_\theta} \right\}^m \right] \qquad \sigma > 0 \qquad (4.49)$$

$$f(\sigma) = 0 \qquad \sigma \le 0 \qquad (4.50)$$

where, $f(\sigma)$ is probability density function. Figs. 4.13 (b) and (d) displays the probability density function $f(\sigma)$ plotted against the unimodular flexural strength and bimodular flexural strength using Eqs. (4.40) and (4.41) respectively for the three-point loading.

Weibull theory correlates the strength distribution parameters based on specimen geometry to a strength distribution parameter based on the material property. The estimated distribution parameters are obtained by taking the logarithm of Eq. (4.47) and after rearranging the expression becomes

$$\ln\left(\ln\left(1/\left(1-P_i\right)\right)\right) = m\ln\left(\sigma\right) - m\ln\left(\sigma_\theta\right) \tag{4.51}$$

Eq. (4.51) is in the form of equation of a straight line, i.e.,

$$Y_i = aX_i + c \tag{4.52}$$

where, $Y_i = \ln\left(\ln\left(1/\left(1-P_i\right)\right)\right)$,

$a = m$ (slope),

$X_i = \ln\left(\sigma\right)$,

$c = m\ln\left(\sigma_\theta\right)$

Using the traditional linear regression, *a* and *c* are obtained from the following expressions:

$$a = \frac{n\sum_{i=1}^{n} X_i Y_i - \sum_{i=1}^{n} X_i \sum_{i=1}^{n} Y_i}{n\sum_{i=1}^{n}\left(X_i\right)^2 - \left(\sum_{i=1}^{n} X_i\right)^2} \tag{4.53}$$

$$c = \frac{\sum_{i=1}^{n}(X_i)^2 \sum_{i=1}^{n} Y_i \; {}_i - \sum_{i=1}^{n} X_i \sum_{i=1}^{n} X_i Y_i}{n\sum_{i=1}^{n}(X_i)^2 - \left(\sum_{i=1}^{n} X_i\right)^2} \tag{4.54}$$

Once '*a*' and '*c*' are estimated from regression, the Weibull parameters *m* and σ_θ can be extracted from the expressions in Eq. (4.51). Graphically the value of *m* is the slope of Eq. (4.51) and σ_θ is the value of tensile strength corresponding to the 63.21% probability of failure.

The Maximum likelihood estimator is also used for determining the value of *m* from a set of fracture strengths. The maximum likelihood estimators (MLE) yield unique solutions for the distribution parameters for a two-parameter Weibull distribution. As the sample size increases, these estimators asymptotically converge to the true distribution parameters and the confidence interval narrows as well relative to other estimators. This latter fact makes this a better choice of the estimation scheme. Let σ_1, σ_2, ….., σ_n represent tensile strength for different experiments (a random variable) in a sample data set, where it is assumed that the tensile strength is characterized by the two-parameter Weibull distribution. The likelihood function associated with this sample is the cumulative probability density evaluated at each of the *'n'* sample values. This likelihood function is dependent on the two unknown Weibull distribution parameters (*m*, σ_θ). The likelihood function, *L*, for an uncensored sample under these assumptions is given by the expression:

$$L = \sum_{i=1}^{n} f(\sigma_i) = \sum_{i=1}^{n} \left\{\frac{m}{\sigma_\theta}\right\} \left\{\frac{\sigma_i}{\sigma_\theta}\right\}^{m-1} \exp\left[-\left\{\frac{\sigma_i}{\sigma_\theta}\right\}^m\right] \tag{4.55}$$

For an uncensored sample data the system of equations is obtained by differentiating the log-likelihood function with respect to m and σ_θ. The derivatives of Eq. (4.55) is equated to zero and represented as:

$$\frac{\sum_{i=1}^{n}\left(\sigma_i\right)^m \ln\left(\sigma_i\right)}{\sum_{i=1}^{n}\left(\sigma_i\right)^m} - \frac{1}{n}\sum_{i=1}^{n}\ln\left(\sigma_i\right) - \frac{1}{m} = 0 \tag{4.56}$$

$$\sigma_\theta = \left(\left(\sum_{i=1}^{n}\left(\sigma_i\right)^m\right)\frac{1}{n}\right)^{1/m} \tag{4.57}$$

Then Eq. (4.56) is solved in an iterative fashion, for estimation of m. Subsequently, σ_θ is estimated from the Eq. (4.57) using the value of m calculated from Eq. (4.56). A closed form solution for the Eq. (4.55) is not available, thus this expression must be solved numerically. The goodness of fit of the Weibull distribution has been determined from estimating the coefficient of determination parameter (R^2). The value of coefficient of determination is found to be more than 0.93 (93%) which might improve by increasing the number of specimens tested. The variation of mean strength determined from all distribution estimators are within a small range. Typically, the value of tensile strength evaluated from the unbiased maximum likelihood estimator for the Weibull two parameter distribution has been further used to find the tensile strength of the flexural graphite specimens.

Fig. 4.13 (b) and 4.13 (d) represents the histogram plot between the frequency (probability density function) and unimodular and bimodular flexural strength of small three-point bend specimen respecively. From all such delineations, it has been observed that the bimodular strength is higher than unimodular strength for

the present case of bimodular ratio greater than unity. The physical significance of the phenomenon is that the material reached failure stress before the classical failure limit when material bimodularity is greater than unity. The Weibull parameters and goodness of fit (R^2) for Weibull distribution estimated through the least square estimator and maximum likelihood estimators for all types of flexural loading (Figs. 4.13 to 4.18) have been tabulated in Table 4.10.

Table 4.10: Comparison of Weibull Parameters and goodness of fit for flexural specimen

Type of Flexural specimens	Weibull modulus for unimodular and bimodular strength			Characteristic Strength						Co-efficient of determination for unimodular and bimodular strength		
				Unimodular			Bimodular					
	LIN2	MLE2B	MLE2U	LIN2	MLE2B	MLE2U	LIN2	MLE2B	MLE2U	LIN2	MLE2B	MLE2U
Small 3-point bend specimen	29.859	28.838	28.140	36.97	37.002	37.002	41.20	41.235	41.236	0.9845	0.9833	0.980
Large 3-point bend specimen	30.470	28.865	27.509	33.38	33.418	33.419	37.20	37.241	37.242	0.968	0.9650	0.956
Small 4-point 1/3 loading	27.866	27.914	27.262	37.39	37.403	37.403	41.66	41.682	41.683	0.9878	0.9878	0.987
Large 4-point 1/3 loading	30.954	28.332	27.001	34.03	34.08	34.082	37.92	37.98	37.981	0.9603	0.9520	0.938
Small 4-point 1/4 loading	29.635	30.466	29.035	37.99	37.991	37.992	42.33	42.338	42.338	0.9851	0.9846	0.982
large 4-point 1/4 loading	30.344	29.722	29.028	34.61	34.618	34.619	38.57	38.579	38.58	0.9642	0.9634	0.963

The six independent sets of flexural strength test data from experimentation are being used in developing Weibull plots to find the Weibull parameters. Fig. 4.13and Fig. 4.14 shows the Weibull statistical analysis plot for the three-point bend small and large specimens with unimodular and bimodular strengths calculated from Eqs. 4.40 and 4.41. Figs. 4.15 and 4.16 also illustrate the unimodular and bimodular strength developed Weibull plot for four-point 1/3

loading for small and large specimens. The similar plot for four-point bend ¼ loading has been plotted for small and large size flexural specimen respectively in Figs. 4.17 and 4.18. The blue dots (Figs a & c) are the actual data sets and the red line represents the linear regression (LIN2) whereas the blue and black line shows the best fit line by maximum likelihood biased (MLE2-B) and unbiased (MLE2-U) estimator. The characteristic strength (σ_θ) and Weibull modulus (m) for flexural specimen have been collected in Table 10 after analysis of plots in Figs. 4.13(a), (c) – 4.13(a), (c). The Weibull modulus (being slope) for unimodular and bimodular strengths are same, however the characteristic strength are distinct as presented in Table 4.10 discretely. The nature of the Weibull plots are found to be similar for unimodular strength and bimodular strength, because the strengths are calculated from the same peak load obtained from the testing via Eqs. 4.40-4.45, so that the coefficient of determination for both the cases are also similar. Understandably, the nature of histogram plot is same; the only difference is the bimodular strength is higher than unimodular strength. This leads to shifting of x-axis (strength) in the Weibull plot without any change of Weibull modulus and coefficient of determination.

4.5 Analytical and Numerical Evaluation of Unimodular and Bimodular Effective Volume

Analytical expressions have been derived earlier for effective volume and also for effective surface in Table 4.1 (a) and (b) respectively. Now, unimodular and bimodular finite element models have been developed and compared with the analytical model to understand the significance of bimodularity on effective volume and hence on the size dependency of strength for bimodular graphite

components. The unimodular finite element results file for various flexural loading condition have been incorporated as input file to the CARES-life program. The CARES natural file so generated stores the data of stress, strain, displacement, coordinates of each and every node for use in reliability analysis and effective volume calculation. The Effective Volume is evaluate using Principal of Independent Action (PIA), in which following expression is implemented for probability of failure

$$P_f = 1 - \exp\left[-\int_V \left(\left(\frac{\sigma_1}{\sigma_0} \right)^m + \left(\frac{\sigma_2}{\sigma_0} \right)^m + \left(\frac{\sigma_3}{\sigma_0} \right)^m \right) dV \right] \tag{4.58}$$

The flow chart mentined in previous chapter Fig. 3.4 describes the calculation procedure of effective volume both for unimodular and bimodular specimens. The experimental unimodular strength based Weibull model using various estimators is followed by Weibpar and CARES-life analysis program (WeibPar V-4.3 and CARES V-9.3) to evaluate the effective volume employing Principal of Independent Action. The evaluated experimental based effective volume has been compared with Quinn's derived effective volume(Quinn 2003b). However, for bimodular effective volume evaluation, program subroutines have been written to calculate the effective volume from the bimodular finite element model. Bimodular strength based Weibull model has been developed using linear regression, biased maximum likelihood estimator and unbiased maximum likelihood estimator. Effective volume (bimodular) has been evaluated from the bimodular FE model using principal of independent action. The effective volume from bimodular strength based experimental model have been compared with the analytical formulation of effective volume derived earlier in Table 4.1 (a) and (b).

4.5.1 Finite Element Model of Bimodular Flexural Specimen

Bimodular finite element model has been discussed in previous chapter 3 in detail. The change of state of stress between two consecutive iterations if remain constant for 99.99% of the assigned nodes, then the iteration is stopped. To lessen the computational time, advantage of parallel processing has been invoked for each bimodular index (Bhushan and Panda 2018). On the basis of above discussion, the bimodular finite element models for the three point and four point bend specimens have been simulated. In order to test the accuracy of finite element results, comparison needs to be made with exact analytical solutions, if available. Alternatively, as the finite element method minimizes a prescribed functional then the solution will converge to the true value with increasing mesh density and therefore, comparison of global response by mesh refinement technique is also an accepted procedure for such convergence studies. As a compromise between solution accuracy and computation time, a grid of 17000 hexahedral elements has been chosen for simulation purpose, as shown in Fig. 4.19. The over-hanging region of the specimens is chosen coarser than the other region of the specimen for enhancing the computational effort without compromising the solution accuracy.

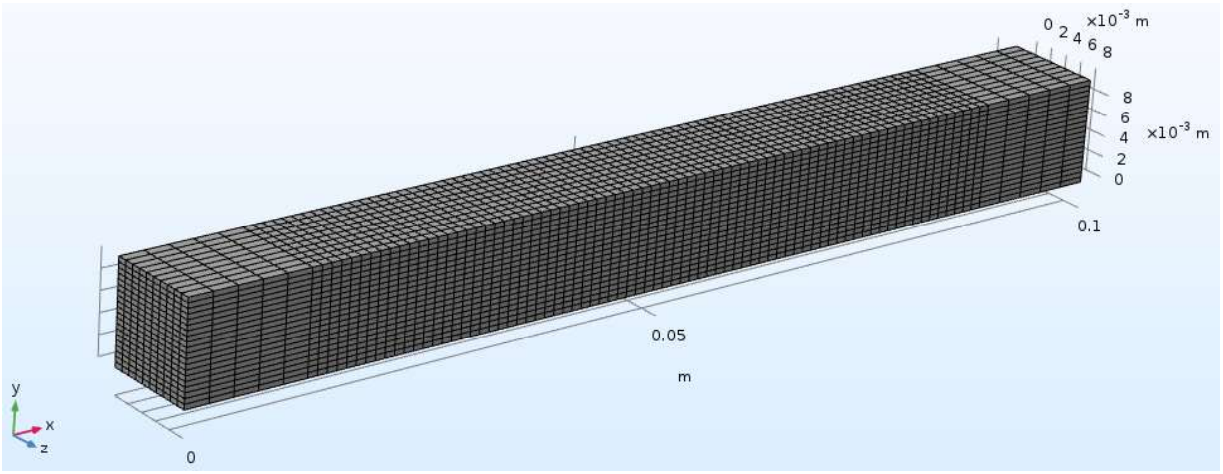

Fig. 4.19. Mesh distribution for finite element analysis

The effect of bi-modularity on stresses, on displacement and on position of neutral surface has been studied from the numerical simulations. The shift of neutral axis and variation of σ_x with respect to the ratio E_t/E_c. for both the problems (three point and four point) have been presented. Fig. 4.20 shows the normal stress distribution in x-direction for three-point bend test and four-point bend test. The results reflect that the maximum value of stress in compression zone is quite high in comparison to tension zone, due to material bi-modularity. For completeness, normal and von-Mises stress distribution has been plotted in Fig. 4.20 and Fig. 4.21 respectively for the three point and four point bend specimens and the non-uniform and asymmetric stress distribution indicate the influence of bimodularity.

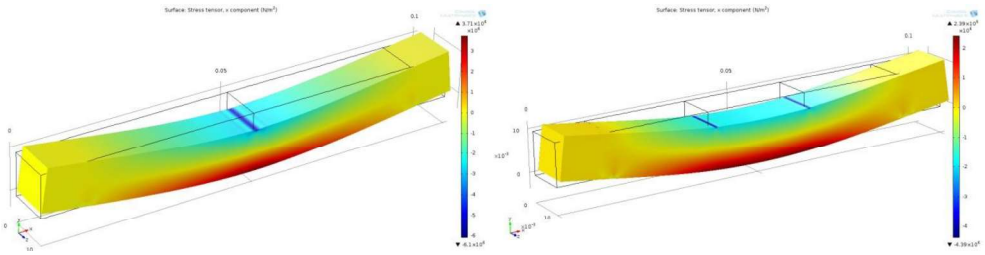

a b

Fig. 4.20. Normal stress distribution in x- direction for (a) three point bend specimen and (b) four point bend specimen

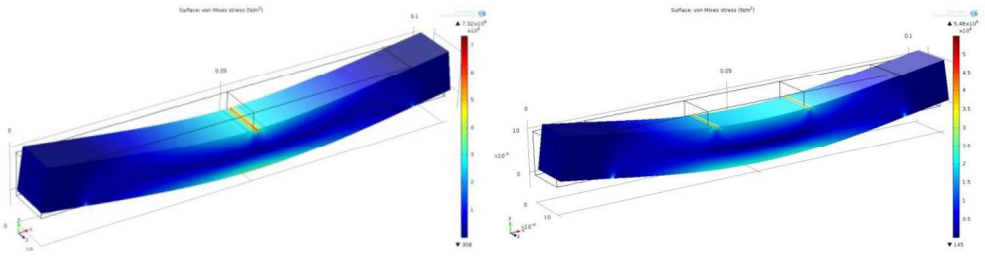

a b

Fig. 4.21. Von-Mises Stress distribution (a) three-point bend specimen and (b) four-point bend specimen

As illustrated in Fig. 4.23, the tension zone is reflected by red color whereas the compression region is reflected by blue color in the 3D geometry of three point bend specimen and four point bend specimen. The shifting of neutral axis has been analyzed by taking a vertical section along the mid span of the three point bend specimen. The shifting of neutral axis at the vertical cross-section has been shown in Table 4.11.

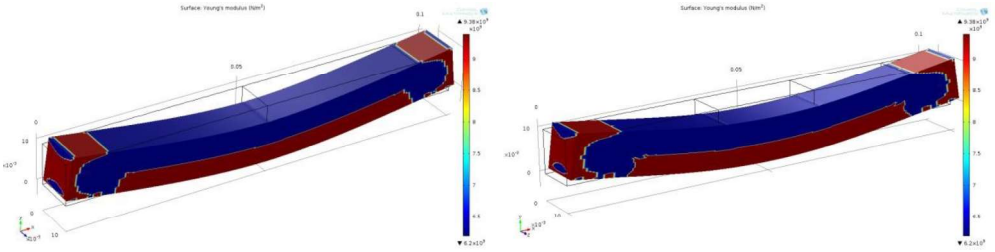

a b

Fig. 4.22 Young's Modulus plot for (a) three point bend specimen and (b) four point bend specimen

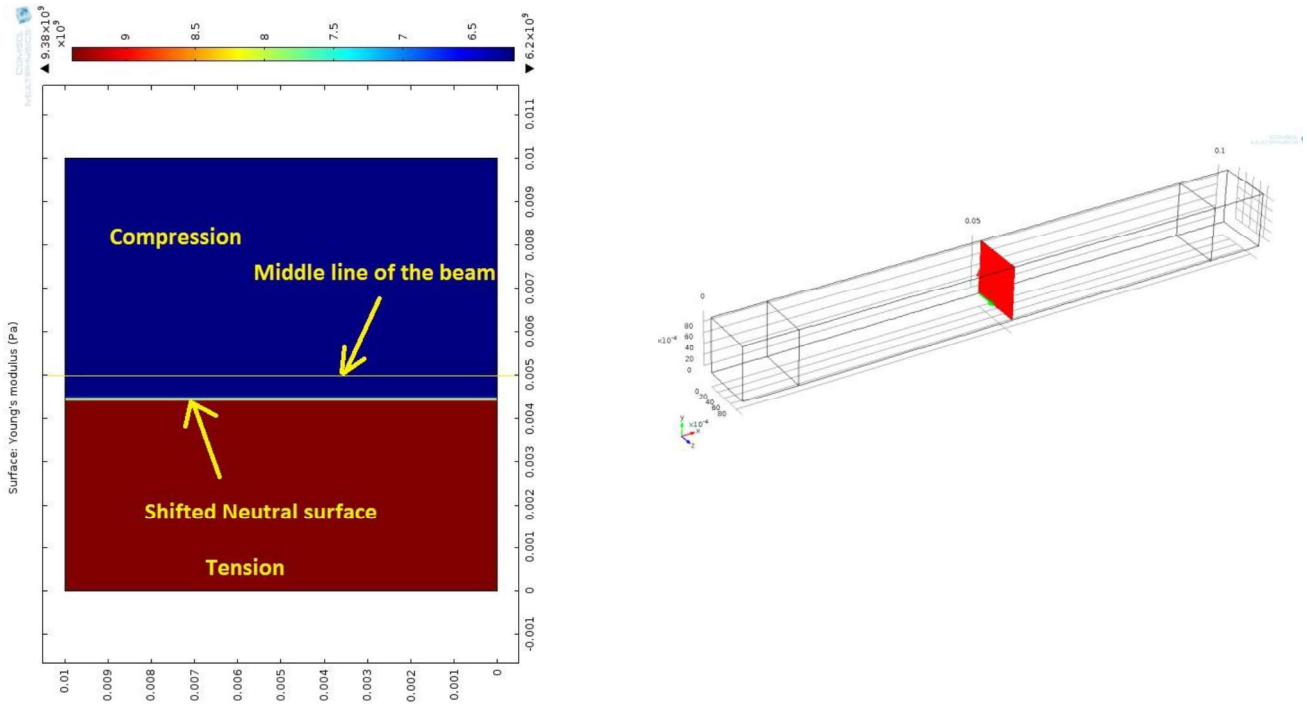

a b

Fig. 4.23 (a)Young's Modulus plot on middle surface of the beam for three point bend specimen and (b) the plane at which the Fig. (a) is plotted

Table 4.11 The results obtained from the three-point bend specimen simulation

Observed neutral axis shift	(in mm)
50mm from the one end	-0.5029
30mm from the one end	-0.5029
Analytical	-0.5163

For determining the neutral axis shift, the normal stress in x direction is plotted against the vertical line shown in Fig. 4.24 (a) at 30mm and 50mm from the location.

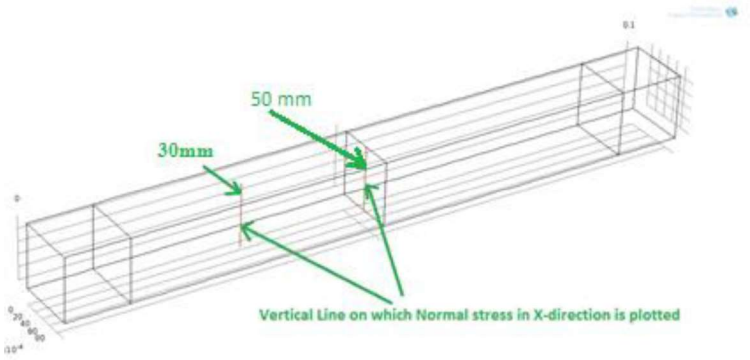

a

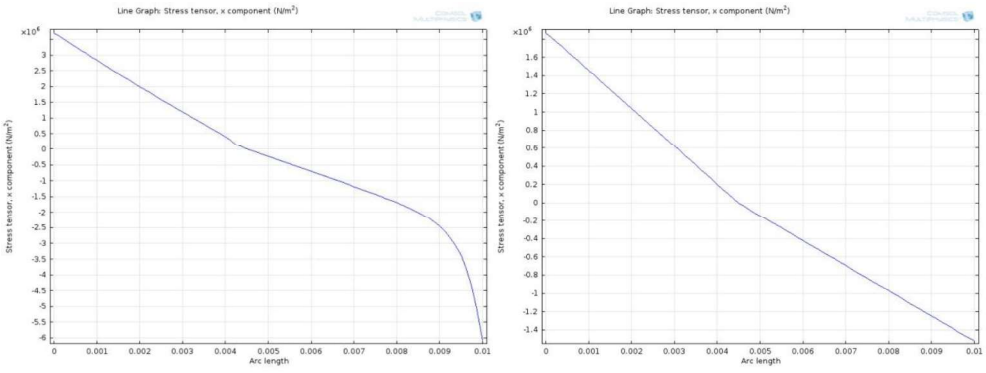

b c

Fig. 4.24 (a) Represent the line in vertical line on which normal stresses in X-direction is plotted (b) 50 mm from left end and (c) 30 mm from left end for three point bend specimen.

The plot for the normal stress in x direction at vertical lines are shown in Fig. 4.24(b) and 4.24(c) at different location. From these plots location of neutral axis and shift from mid surface can be easily evaluated. This explains the variation of observed strength in test specimens with unimodular and bimodular assumptions.

Fig. 4.25 shows the neutral axis shift for the beam subjected to three point and four point 1/4 loading condition for a range of E_t/E_c ratio and results were compared with the analytically calculated results. Finite element simulation

results are found to consistently match with the analytical solution for neutral axis shift.

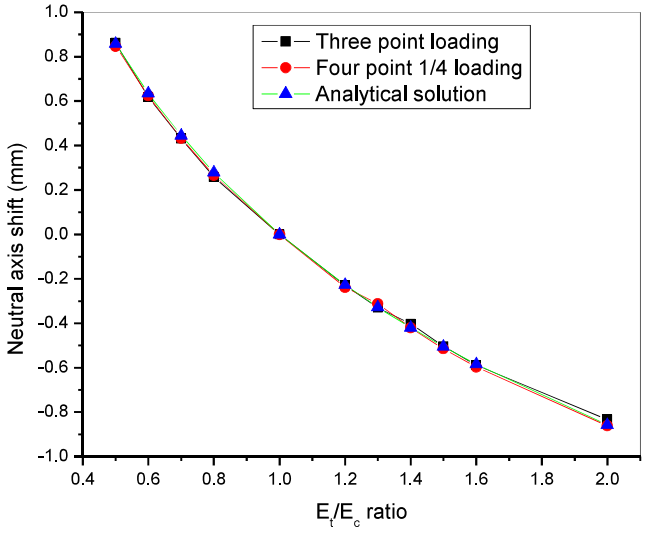

Fig. 4.25 Neutral axis shift for a range of E_t/E_c ratio for three point bend specimen at the 30mm from left end of the beam

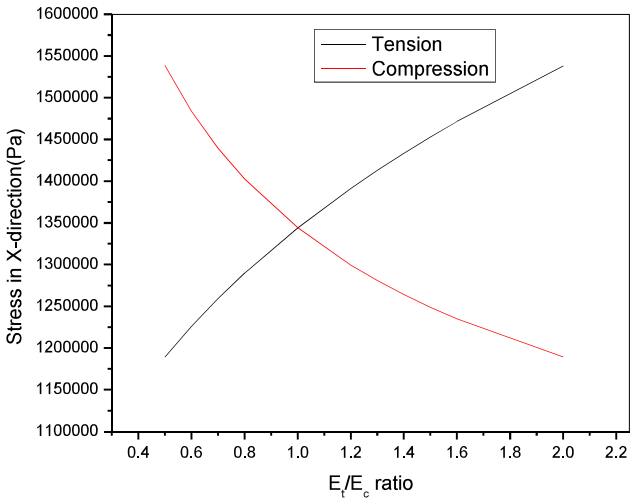

(a)

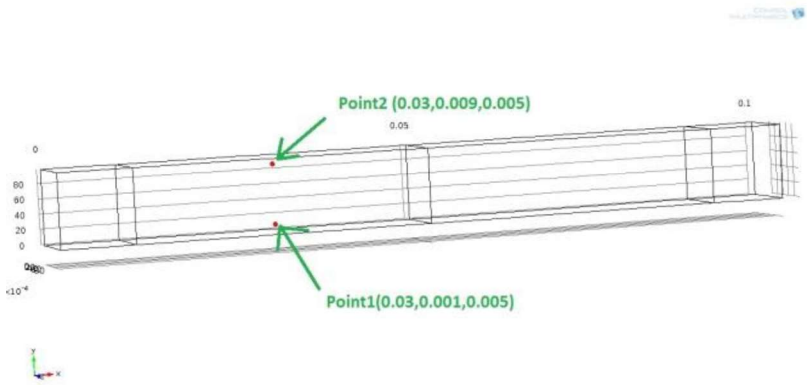

(b)

Fig. **4.26** (a)Variation of σ_x for a range of E_t/E_c ratio in three point bend specimen, (b) the two points in compression and tension are located in specimen.

Finally, Fig. 4.26 represents the variation of σ_x at the two points on vertical section at 30mm from left end and positioned at 1mm from top and bottom surface of the beam for different E_t/E_c ratio for three point loading condition. It is reflected from the figures that the σ_x in tension increases with increase in E_t/E_c ratio, whereas in compression it decreases. The bimodulus ratio E_t/E_c has strong influence on both neutral axis shifting and the axial stress distribution. This can be stated here that the evaluation of effective volume and size dependence might lead to susceptible structures resulting in catastrophic failures if bimodular behavior is ignored in the analysis. So also in the present study, post processing codes have been written in Fortran language to evaluate the bimodular effective volume by taking the input from developed bimodular FE model. The flow chart in Fig. 3.3 has already discussed the process of evaluating effective volume in unimodular and bimodular cases. These values obtained from analytical and numerical FE model has been noted in Table 4.12 for all loading cases for a comparative analogy of influence of bimodularity.

Table 4.12. The unimodular and bimodular *effective volume* estimated with analytical derived expression and FE model for the flexural graphite specimens.

Specimen Type	Analytical			By mathematical (FE) model			Analytical			By mathematical (FE) model		
	Effective Volume For Bimodular material (mm^3) derived in this manuscript			estimated Effective Volume For Bimodular material (mm^3)			Effective Volume For Unimodular material (mm^3) (Quinn 2003b)			estimated Effective Volume For Unimodular material (mm^3)		
	LIN2	MLE2B	MLE 2U	LIN2	MLE2B	MLE 2U	LIN 2	MLE 2B	MLE 2U	LIN 2	MLE 2B	MLE 2U
Small 3-point bend specimen	3.76	4.031	4.227	3.734	4.213	4.443	4.200	4.492	4.710	4.20004	4.4927	4.7106
Large 3-point bend specimen	56.62	62.879	69.00	56.942	63.093	69.875	63.105	70.073	76.896	63.106	70.073	76.896
Small 4-point 1/3 loading	43.21	43.13	44.19	43.563	44.373	44.983	48.155	48.070	49.251	48.156	48.07	49.252
Large 4-point 1/3 loading	606.1	663.7	697.432	606.243	665.763	697.432	675.46	739.718	777.225	675.47	739.72	777.22
Small 4-point 1/4 loading	60.4	58.84	61.741	60.989	59.658	62.234	63.642	60.425	64.876	63.843	60.219	64.822
large 4-point 1/4 loading	923.1	942.4	964.939	923.458	943.243	965.456	1048.172	1004.270	1005.085	1048.3	1004.7	1005.1

The post-processing code takes the input results from FE bimodular model simulation for the validation of bimodular graphite fracture data and the values are tabulated in Table 4.12. The bimodular analytic effective volume described in the first three columns of the Table 4.12 has been calculated with least square, maximum likelihood biased and unbiased estimators from the bimodular experimental test data of the flexural specimens using derived expression presented in Table 4.1 (a) and (b) in this manuscript. The next three columns are estimated from self-developed program which employs the bimodular FE model post processing results. Next three columns are unimodular effective volume of flexural specimens. The remaining three columns data set for the effective volume has been obtained from the unimodular FE model with Weibpar and CARES post processing. The effective volume of flexural specimen tested in three-point loading has been found to be comparatively close for analytical and mathematical

model with unimodular material assumption. In retrospect, the effective volume calculated from the bimodular FE model based post-processing code has been very close to the bimodular effective volume as calculated from expressions presented in Table 4.1 (a). The more generalized material model is bimodular model which has been validated with experimental based FE model.

4.6. Conclusions

The structural integrity assessment of high risk ceramic and graphite components have been dubious and unreliable due to the inherent material bimodularity. The testing, evaluation and prognosis of such components pose an uncertainty of scattered damage accumulation patterns leading to catastrophic brittle fracture. Therefore, probabilistic methods have evolved as an ultimatum to study their operational and functional transients. In the present work, Weibull effective volume and surface area analytical expressions for beam of rectangular and square cross section possessing bimodularity and loaded in different flexural configuration (1. Uniform bending; 2. Three-point bending; 3. Four-point General 4. Four-point,1/4 point 5. Four-point,1/3 point) have been derived and tabulated. Extensive experimentation for flexural graphite specimens with configurations viz.: Small 3-point bend specimen, Large 3-point bend specimen, Small 4-point 1/3 loading, Large 4-point 1/3 loading, Small 4-point 1/4 loading and large 4-point 1/4 loading have been carried out to quantify influence of bimodularity and size dependence on strength. Weibull analysis of the fracture strength test data for all specimens have been conducted to evaluate Weibull modulus and characteristics strength with unimodular and bimodular quantification. Analytical and finite element models for the unimodular and bimodular specimens have been

compared with Weibull effective volume as the characterizing parameter for studying the size dependence on strength.

In a bi-modular beam, neutral axis is shifted from centroidal axis and thereby volume in tension and maximum tensile stress in the specimen are different as compared to the unimodular case and thus causing changes in the Weibull effective volume. Strength scaling ratios for bimodular beam is also different from the unimodular beam, which might depend on whether the flaws are volume or surface distributed for the beams having same cross-section. Conversion factors have also been tabulated for different flexural loading configurations. The analytical expressions, Weibull effective volume and effective surface area have been tabulated for easy referral for a qualitative comparison between specimens having large offset in dimensions as with respect to laboratory and real scale models. Significant variations with unimodular and bimodular preclusions demonstrated in this work explains the uncertainties observed in the failure mechanism of components designed with unimodular concepts which seemingly might have been more appropriate if bimodularity would have been considered.